

# Design and Field Testing of a Rover with an Actively Articulated Suspension System in a Mars Analogue Terrain

Florian Cordes\*, Frank Kirchner\*<sup>†</sup>, and Ajish Babu\*

Reformatted version. Original version in: *Journal of Field Robotics* ©John Wiley & Sons, Inc. 2018  
<https://onlinelibrary.wiley.com/doi/abs/10.1002/rob.21808>

This article presents the electro-mechanical design, the control approach and the results of a field test campaign with the hybrid wheeled-leg rover SherpaTT. The rover ranges in the 150 kg class and features an actively articulated suspension system comprising four legs with actively driven and steered wheels at each leg's end. Five active degrees of freedom are present in each of the legs, resulting in 20 active degrees of freedom for the complete locomotion system. The control approach is based on force measurements at each wheel mounting point and roll-pitch measurements of the rover's main body, allowing active adaption to sloping terrain, active shifting of the center of gravity within the rover's support polygon, active roll-pitch influencing and body-ground clearance control. Exteroceptive sensors such as camera or laser range finder are not required for ground adaption. A purely reactive approach is employed, rendering a planning algorithm for stability control or force distribution unnecessary and thus simplifying the control efforts. The control approach was tested within a four week field deployment in the desert of Utah, USA. The results presented in this paper substantiate the feasibility of the chosen approach: The main power requirement for locomotion is from the drive system, active adaption only plays a minor role in power draw. Active force distribution between the wheels is successful in different footprints and terrain types, and is not influenced by controlling the body's roll-pitch angle in parallel to the force control. Slope climbing capabilities of the system were successfully tested in slopes of up to 28° inclination, covered with loose soil and duricrust. The main contribution of this article is the experimental validation of the actively articulated suspension of SherpaTT in conjunction with a reactive control approach. Consequently, hardware and software design as well as experimentation are part of this article.

## 1 Introduction

Nature provides a vast amount of examples that legged, walking or climbing locomotion is an excellent means to cover even the steepest cliffs and to reach literally any place on a planetary surface. Goats climbing steep rocky surfaces, Geckos with adhesive feet managing smooth surfaces or many types of insects are only a few examples of impressive locomotive capabilities to be found in the animal domain.

In the robotic domain, walking robots are of increasing interest as for example shown at the Darpa Robotics Challenge (DRC) (Krotkov et al., 2017). The majority of robots taking part in the DRC finals were walking robots, most of them in some kind of humanoid form. Despite the high number of walking robots in the contest, and recent advances in developing walking and climbing robots, most of the highest ranked systems in the challenge were those combining walking and driving locomotion in one way or the other. This contest's result illustrates the advantages of combining different modes of locomotion in a robotic system and adapting the locomotive system according to the current task and environment.

Looking into the application area of space robotics, all

mobile robots deployed for exploration of celestial bodies are up to now purely wheeled systems, equipped with a performant passive suspension system, yet without the possibility to adapt the locomotive system to a wider range of terrain types or non-nominal situations (sinkage in soft soil, getting entangled between rocks or alike). The employed systems provide the possibility to carry scientific instruments to locations several kilometers away from the landing spot (Lindemann and Voorhees, 2005) (Volpe, 2005). However, new mission scenarios with additional requirements concerning sample return, sites to take samples from and their reachability with robotic systems as well as improved fault-recovery abilities demand for new solutions.

The approach presented in this paper is to combine benefits of the domain of legged locomotion with those of the domain of wheeled locomotion to form an active suspension system (Cordes and Babu, 2016), (Cordes et al., 2017). As a result the hybrid wheeled-leg rover *SherpaTT* was designed, integrated and tested. In this paper the rover system is presented in terms of electro-mechanical design, control approach and testing within a field test campaign during October and November 2016 in the desert of Utah, USA. The extensive experimental validation in a field deployment is the main contribution of this paper. Several aspects of the chosen test site are good representatives of terrain on Mars, including segmented and inverted river beds that can be found on Mars, providing a potential source of astrobiological data, (Clarke and Stoker, 2011). Due to the geological similarity other Mars analogue tests were con-

\*DFKI Robotics Innovation Center Bremen, Bremen, Germany [firstname.lastname@dfki.de](mailto:firstname.lastname@dfki.de)

<sup>†</sup>University of Bremen, Faculty 03: Mathematics/Computer Science, Bremen, Germany



Figure 1: The hybrid wheeled-leg rover SherpaTT during the field test campaign. In the photograph, the system is equipped with modular units used in a multi-robot scenario. The two antennae of the DGPS-system used for ground truth-data can be seen behind the central manipulator.

ducted in the area as well, (Dupuis et al., 2016), (Caudill et al., 2016), (Gingras et al., 2017).

Figure 1 shows the final design of SherpaTT as deployed in the field test campaign with connected modular payload-containers. During the field tests, locomotion experiments, navigation and autonomous control tests and a multi-robot sample-return mission were conducted. This article focusses on the suspension design and the locomotion experiments conducted with SherpaTT during the field tests. An overview on the experiments conducted and general field experiences are presented in (Sonsalla et al., 2017).

We define the following terms as used throughout the paper:

*Definition 1.1: Wheeled-Leg.*

In this paper, a *wheeled-leg* is considered as a limb of a robot that, instead of a foot for ground contact, makes use of a wheel at the ground contact point. Alternatively the term *wheel-on-leg* can be found in literature.

*Definition 1.2: Leg End Point (LEP).*

The term *LEP* in this article is used to kinematically describe a wheeled-leg of a robot. A LEP is considered to be the idealized point of contact of a rigid wheel on rigid ground. The location of a LEP is considered to be described by a vector in cartesian coordinates  $p = (p_x \ p_y \ p_z)^T$  or cylindrical coordinates  $p = (p_\alpha \ p_r \ p_z)^T$ . Currently, the LEP is used as reference for controlling the active ground adaption, see Section 5.

*Definition 1.3: Wheel Contact Point (WCP).*

The real contact point between wheel and ground might be different from the LEP and is defined as the *WCP*. A wheel can have more than one WCP or no WCP when the wheel is lifted off the ground, but there is always exactly one LEP. In a further advanced control, the ground adaption would react to the WCP(s) and not the LEP.

The remainder of this article is structured as follows. The following chapter gives an overview of the related

work. This encompasses passive and active suspension system rovers and a comparison of benefits and drawbacks of both approaches. Chapter 3 gives an overview on the full rover system, while the mechanical design and kinematics analysis of the system is detailed in Chapter 4. The control approach of the suspension system and how to take advantage of the kinematic structure for locomotion is described in Chapter 5. With Chapter 4.4 a brief discussion on the effect of individual joint failures and other operative risks is provided. Chapter 6 focusses on the experiments conducted with SherpaTT and the results and conclusions from these experiments. The article closes with lessons learned and a summarizing conclusion in Chapter 7.

## 2 Rover Suspension Systems: Passive vs. Active

One means of exploration of celestial bodies is remote sensing, for example with satellites passing or orbiting a planet or moon. A more direct approach is a lander equipped with a robotic arm, like the Phoenix lander (Smith, 2004). Such stationary units can provide data in the direct vicinity of the landing spot, for example by soil sampling and analysis with appropriate instruments on the landing unit. Depending on the type of lander, propulsion plumes might contaminate the direct vicinity of the landing spot and thus if not rendering impossible at least complicate the interpretation of data from soil samples. To gather data from “in-situ” measurements at multiple locations on a celestial body’s surface with more distance to the landing spot, mobile robotic devices are required.

### 2.1 Passive Suspension Systems

Recently deployed mobile robots on Mars (Mishkin et al., 1998), (Lindemann and Voorhees, 2005), (Welch et al., 2013) or China’s Yutu-rover from Chang’e 3 mission to Moon feature wheeled locomotion with passive adaptive suspension systems. All these rovers are equipped with a suspension system known as *rocker-bogie* suspension (Bickler, 1989), (Harrington and Voorhees, 2004). Two identical linkage mechanisms are fixed on either side of the rover, connected via a differential. Each linkage consists of a rocker which has one wheel mounted on the front end of the vehicle and a bogie with two wheels pivoting at the rear end of the rocker. The effect of the connecting differential between the two rockers is that the pitch angle of the rovers’ body maintains the average angle of the two rocker angles. The size of negotiable obstacles is related to the wheel size. A rover with a rocker-bogie suspension can typically overcome obstacles of a height in the range of a wheel’s diameter: The MER systems have a wheel diameter of 25 cm and are stated to safely traverse obstacles of 25 cm height (Lindemann and Voorhees, 2005).

Similar to a rocker-bogie suspension is a mechanism known as triple bogie or 3-bogie configuration as found in the ExoMars rover (Michaud et al., 2008). One bogie

with two wheels is mounted on the left, right and rear of the robot in this type of suspension configuration. No differential or other connection is present between the single bogies, the rear bogie acts as a leveling mechanism for roll angles. Apfelbeck et al. (Apfelbeck et al., 2011) report on obstacles that might get the rover stuck, yet most test-cases showed a good terrain performance of this passive suspension system. A triple bogie configuration with supporting spring elements is presented in (Manz et al., 2014).

Another bogie configuration can be found in the CRAB rover (Thueer et al., 2006). As opposed to the rocker-bogie or triple bogie configuration, a symmetrical design with two parallelograms attached to one rocker is chosen for this system. A further passive suspension is shown for example in the rovers Shrimp (Lamon and Siegart, 2003) and SOLERO (Michaud et al., 2002) which are six-wheeled rovers with two wheels on each side central body and one wheel in the front and one wheel at the rear end of the rover.

All the above mentioned passive suspension systems are designed to keep all wheels in ground contact and to equally distribute loads between the wheels. Furthermore, the roll and pitch angles of the rover bodies are reduced by the design of the suspension when compared to fixed suspension in equally sloping terrain. A clear benefit of these systems is that no active control of linkages is needed, the kinematics of the passive suspension ensure optimal ground contact in most situations.

However, certain stuck situations are reported from which the rover cannot free itself. This is a clear drawback of a passive suspension system. Furthermore, the body angle with respect to gravity can not be influenced arbitrarily. For climbing obstacles, enough traction is required to be able to push a wheel up an obstacle. In cases with low ground traction, the rover might fail to overcome the obstacle.

## 2.2 Active Suspension Systems

Wilcox et al. (Wilcox et al., 2007) argue that using wheeled-legs for propulsion creates the possibility to walk out of stuck situations. Additionally, a wheel can be actively lifted to climb an obstacle, reducing the risk of entangling robot structures with the obstacle. Unlike in passive suspension, the wheels remaining on the ground do not need to provide thrust to push a wheel up an obstacle. This bears the potential for better obstacle negotiation in slopes: slippage of wheels compromises the thrust needed in passive suspension to push the wheel onto the obstacle.

When a rover can walk out of a stuck situation, the wheel torque requirements can be relaxed: For dimensioning a wheel's actuator, a worst-case scenario where one wheel is stuck in a hole and the rover is tilted onto that wheel can be assumed. This load case implies that the wheel needs to generate a torque that allows to push half of the rover's mass vertically up (Wilcox, 2012). If the suspension system can actively pull the wheel out

of the stuck situation the peak thrust requirement for each wheel can be reduced. Reducing the peak thrust allows to reduce the gear-box size and hence reduce the weight of the actuator. Additionally, the motors can operate closer to their specific working point, since the ratio between thrust in nominal operation and in worst-case operation is significantly smaller. Combined with the reduction of the wheel size due to reduced requirements for ground pressure limits, a wheeled-leg system can be about 25% lighter compared to an alternative all-terrain mobility system (Wilcox, 2012). Hence, combining legs and wheels to wheeled-legs has the potential to combine the benefits of both, walking and driving locomotion.

Active suspension systems, depending on their design can further reduce the overall system mass which includes the lander system: Using such a suspension can render ramps or other rover deployment systems unnecessary (Haarmann et al., 2012) (Townsend et al., 2010). At least an increase in safety for lander egress when using ramps can be achieved using active elements in a suspension as shown in (Azkarate et al., 2015).

A combination of walking and rolling motion using the deployment actuators of ExoTeR (ExoMars Testing Rover) showed increased performance when compared to only rolling motion in three different experimental scenarios, namely freeing from a stuck situation in soft soil, up-slope capabilities and lander egress (Azkarate et al., 2015). The ExoTeR makes use of a triple bogie suspension as the ExoMars platform does. Furthermore, each wheel has a deployment actuator, that is responsible for the transition of the folded stow configuration to the unfolded driving configuration after the landing manoeuvre.

Another system combining active and passive suspension is the Scarab rover (Bartlett et al., 2008). Passive terrain adaptability is achieved by a differential rocker mechanism connecting the two rockers on each side. The opening angle of each of the two rockers can be set with an actuator, providing two active Degrees of Freedom (DoFs) in the suspension system. In (Wettergreen et al., 2009) the outcome of field testing the Scarab rover is presented.

Similar in suspension design to Scarab is the Sample Return Rover (SRR), which has four wheels that are mounted on a similar two-rocker system with controllable shoulder joints. As opposed to Scarab the wheels can be independently steered, allowing explicit steering maneuvers. In (Iagnemma et al., 2003) the SRR rover demonstrates improved terrain stability when roving in undulating terrain with active adaption of the suspension system.

A rover with an actively actuated suspension designed for lunar mission is the ATHLETE rover (Wilcox et al., 2007) (Heverly et al., 2010). The ATHLETE family of rovers employs an actively articulated suspension composed of six limbs with six Degree of Freedom (DoF) each. Each limb can be used as a general purpose manipulator with a tool adapter. The size of of a ATHLETE

SDM rover is 2.75 m in diameter with a total mass of 850 kg.

In (Reid et al., 2016) a rover with an actively articulated suspension system is presented. The rover has four wheeled-legs with four active DoF each. The ground adaption strategy is based on a planned trajectory for the rovers body. With the terrain information gathered from a RGB-D sensor, joint movements in the limbs are planned that lead to the desired body trajectory in unstructured terrain.

The rover SherpaTT presented in this paper is a system that fits into the category of active suspension systems described in this section. In contrast to the systems described above, SherpaTT has a six-axis force-torque sensor mounted at each wheel, allowing a direct measurement of the interaction with the ground. A force estimation using joint displacements or joint currents is not required, which in turn allows the employment of self-locking gears that do not need to be powered to keep the current position. Apart from flexible metal wheels (Kroemer et al., 2011), no passive suspension is implemented in SherpaTT. The reactive control approach implemented in SherpaTT (Cordes et al., 2017) together with the chosen workspace of the legs of the suspension system allow for active ground adaption during a continuous drive in sloping terrain. A sequential “drive-stop-adapt” motion strategy is not necessary.

### 2.3 Conclusion

Above examples show that passive suspension systems as employed or envisioned for current space exploration robots provide good terrain traversability in many cases. However, limits of these systems occur in steeper slopes covered with obstacles and in non-nominal situations, especially in cases where a robot gets stuck in soft soil. Actively articulated suspension systems bear the potential to increase the rover’s locomotive capabilities and hence increase the margin before reaching non-nominal states or increase possibilities to recover from non-nominal system states.

The additional actuators required for active suspension do not necessarily increase the system mass as savings in actuator size and – having the full space system in mind – lander system are possible due to the increased capabilities of the mobile robot (Wilcox, 2012) (Townsend et al., 2010) (Haarmann et al., 2012).

However, it is clear that any active element in a suspension system needs an input (i.e. sensors) and a control strategy, hence processing power, to be able to actively adapt to the terrain at hand. In many cases simple strategies already show improvements in active locomotion (Haynes et al., 2017), reducing the computational and sensory requirements. The strategy pursued for SherpaTT and presented in this article relies basically on four force measurements at the wheels as well as roll and pitch measurements of the body as the only exteroceptive data for ground adaption. No terrain models are employed, a purely reactive control approach is pursued.



Figure 2: Multi-Robot Scenario: SherpaTT is handing over a sample container to CoyoteIII for return to the lander. CoyoteIII has the modular manipulation arm SIMA attached which is currently in a pose to facilitate the container hand-over.

## 3 SherpaTT: System Overview

The rover SherpaTT is a four-wheeled mobile robot with an actively articulated suspension system and a manipulation arm. The five limbs of the system add up to 26 active DoF in total, five in each of the four legs and six DoF in the manipulator arm. Apart from the active suspension system, a modular system approach with exchangeable Payload-Items (PLIs) is another key feature of the rover. Figure 2 shows SherpaTT during a multi-robot system test. Details on the modularity and the multi-robot scenario can be found in (Roehr et al., 2014), (Sonsalla et al., 2014), (Wenzel et al., 2015), (Sonsalla et al., 2017).

SherpaTT is the successor of the system Sherpa (Cordes et al., 2011) improving the workspace of the legs while having a reduced number of active DoF (Cordes et al., 2014). Both Sherpa-versions are designed to work together with other robots in unstructured terrain; while Sherpa has to transport a highly mobile six-legged walking robot (Roehr et al., 2014), SherpaTT has to transport immobile payloads requiring a higher flexibility in the rover’s body pose control for deployment and pick-up. Compared with the design of the predecessor Sherpa, SherpaTT’s suspension provides a three- instead of two-dimensional positioning of the LEP by introducing a second parallelogram in the leg and thus creating a “knee”.

Overall, SherpaTT has a mass of 166 kg and a payload capacity of at least 80 kg. Each of the four suspension system units (legs) has a weight of 25.75 kg, the manipulator arm has a mass of 25 kg and the central body including the manipulator mount and the mounts for the Electro-Mechanical Interfaces (EMIs) has a mass of approximately 38 kg excluding batteries. The payload capacity results from a fully equipped system with two PLIs in each of the four available payload-bays, a Base-Camp mounted beneath the robot (15 kg) and a 25 kg mobile robot lifted with the manipulator arm. The rover can vary its support polygon spanned by the four Leg End Points (LEPs) between one square meter in stow pose with a 1 m×1 m footprint and around six square

meters with fully stretched legs spanning a  $2.4\text{ m} \times 2.4\text{ m}$  polygon.

The main power supply consists of two 44.4 V Lithium Polymer batteries with 10 Ah each. A power management system switches autonomously between the two batteries, an external power supply or power from the modular bus when a battery module is present. The priority is (1) external power supply (2) internal LiPo-batteries (3) attached battery module. Table 1 lists the key system specifications of the rover system, including dimensions, mass and performance characteristics.

Currently, a standard i7 PC running Linux is used for locomotion and high level control implementation. Motion control and high level processes for navigation and planning are implemented using the Rock<sup>1</sup> framework.

## 4 System Design

This chapter describes the mechanical design of the rover SherpaTT with a focus on the suspension system. The methodology for actuator selection is highlighted. For completeness, the manipulation arm is briefly introduced as well.

### 4.1 Kinematics of the Suspension System

Figure 3 shows the final design of a leg with annotations for DoFs and the placement of a six-axis force-torque sensor. The suspension system of SherpaTT consists of four identical legs ending in a drivable and steerable wheel. Each of the legs has five active DoF in total. Three out of the five DoF are used for placing the LEP in three dimensions relative to the body. The two outermost DoF are used to orient the wheel for steering and to drive the wheel, respectively. Figure 4(a) provides the definition of the leg index (starting with  $i = 0$  at front left leg), and shows a schematic of the Pan joints angle  $\alpha = 0$ . The zero positions of InnerLeg  $\beta$ , OuterLeg  $\gamma$  and WheelSteering  $\varphi$  are provided in Figure 4(b).

The linear drives responsible for the movement of the parallelograms are mounted such that the weight of the robot pulls on the actuator, hence undesired bending forces from pushing the linear drive are avoided. The WheelSteering joint is placed over the center of the wheel, avoiding a movement of the wheel on a circular path around the joint's axis during a steering manoeuvre. Furthermore, the WheelSteering actuators are not experiencing loads from WheelDrive torques.

Figure 5 illustrates the workspace of the rover's suspension system. Rotating the Pan joint creates a circular path of the leg's LEP around the joint's rotational axis which is also defined as the z-axis of the Leg Coordinate System (LCS). Movements with InnerLeg and OuterLeg joints allow to control the distance of the wheel to the LCS origin as well as the height of the wheel w.r.t. the body. Combining all three joints creates the toroid

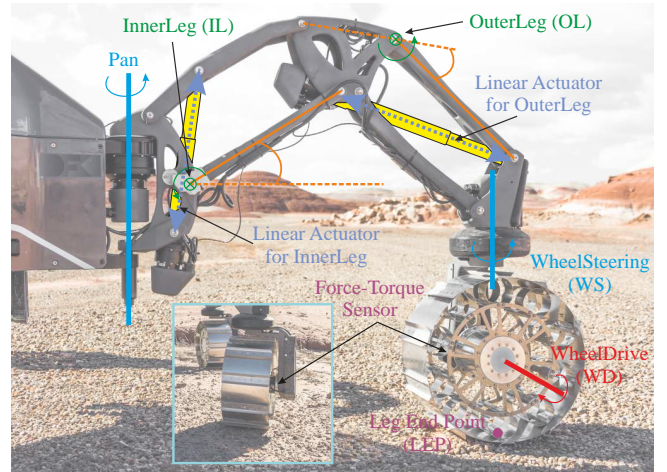
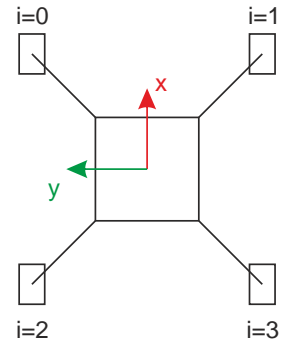
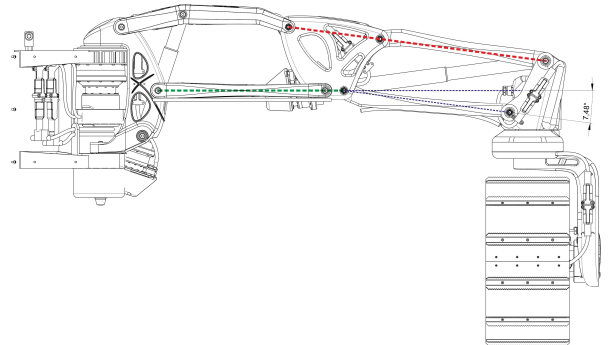


Figure 3: Description of DoF present in SherpaTT's suspension system and placement of force-torque sensor.



(a) Leg index and zero position of Pan joint  $\alpha$ . Top view.



(b) Definition of zero positions. Note that OuterLeg zero position is not defined as horizontal.

Figure 4: Kinematics: Joint positions and leg indexing.

<sup>1</sup>Robot Construction Kit <http://rock-robotics.org>

Table 1: SherpaTT System Specifications

Parameter Name	Value	Comments
<b>Performance Characterization</b>		
Step & Obstacle Height	0.772 m	Active stepping necessary for step-like obstacles
Ground Clearance	0.10 m – 0.80 m	Variable, can be commanded
Locomotion Speed	0.1 m/s (nom) 0.7 m/s (max)	Currently limited by software to 0.2 m/s
Turning Arc (circular wheel path)	1 m (min) 2.1 m (nom)	Wheel track radius with point turn Point turn in nominal suspension configuration
<b>Dimensions</b>		
Foot Print Size	variable from 1 m <sup>2</sup> to ≈6.76 m <sup>2</sup>	Smallest footprint: a square with 1 m edge length. Biggest: 2.6 m edge length. Arbitrary non-symmetric foot prints possible (Cordes et al., 2011) (Cordes and Babu, 2016)
Leg Length as distance between Leg Pivot (Pan) and LEP	1.082 m 0.880 m	Fully stretched leg Nominal configuration: PoseA in Figure 5(c)
Number of active DoF	26	4×5 suspension system, 1×6 arm
<b>Masses</b>		
System Mass $m_g$	166 kg	Total mass, w/o payloads, w/o batteries
Thereof: Legs	25.75 kg	(×4)
Thereof: Arm	25 kg	
Thereof: Central Body	38 kg	Includes structure, electronics, hull, arm mount, EMI mounts
Payload Capacity	≈ 80 kg	Based on 4×2 PLI with 5 kg/ in payload bays, one BaseCamp with 15 kg and a 25 kg payload at the manipulator.
<b>Power-Supply</b>		
Internal DC-Power	2× 44.4 V/10 Ah	Autonomous switching from empty to full battery
External DC-Power	50 V / 20 A	External AC/DC-converter with power tether
Nominal Power	≈150 W ≈200 W/225 W/250 W	Base load $P_b$ of processors, DC/DC converters, sensors etc Total mean power when driving in flat/moderate/steep terrain. Peak loads up to 350 W possible.
<b>Sensors</b>		
Lidar	Velodyne HDL-32E	Main navigation sensor. Sensor mount rotates with first manipulator arm joint.
Laser Range Finder	Hokuyo UST-20LX	Tiltable. Mounted on front face. Used mainly for manipulation purposes.
Camera	Allied Vision GC1380	1360×1024px, 20.2fps, 12bit, CCD camera for human operator. With Fisheye lens Fujinon FE185C086HA-1
Attitude and Heading Sensor	Xsens MTi-300	
Force Torque Sensors (Legs)	FT-DELTA 160	Mounted at each wheel for autonomous ground adaption
Force Torque Sensor (Arm)	FT-mini 45	Part of manipulation interface
Joint Level Sensors		Current (total and phase), voltage, speed, position, temperature
<b>Communication</b>		
External Wireless	2.4 GHz (802.11n)	WiFi
External Cable Connection	GbE	Ethernet switch connected to WiFi, control PC and modular interfaces
Internal Joint Communication	NDLCom via LVDS	Custom protocol / inter-hardware communication
Remote Emergency Switch	868 MHz Xbee-Pro	Custom hardware
<b>Modularity / Interfaces</b>		
Passive EMIs	4×	Mounted as “payload-bays” around arm mount
Active EMIs	2×	Mounted below central body and used as manipulation interface
Power Bus via any EMI	44.4 V / 10 A	Bi-directional power transfer possible
Ethernet via any EMI	100Mbit/s	4Pin Fast Ethernet
Local Communication	RS422	Between Modules, i.e. for organization of topology

shown in Figures 5(a) and 5(b). The toroid is the leg’s workspace in which the LEP can be positioned relative to the body.

Figure 5(c) displays a cross-section of the workspace with indications for preferred poses of the leg. The nominal robot configuration is named Cross-Stance and has the LEPs at PoseA together with  $\alpha = 0$ . In this nominal configuration, the vertical stroke of the LEP is 671 mm, without changing the distance to the body. Pose B is a compromise between maximizing the possible body height and still having a feasible vertical stroke, while Pose C is the distance of the LEP to the leg coordinate origin that allows the highest body configuration. The total vertical stroke is 775 mm when moving the LEP from PoseA-up to PoseC-down. Note that the defined preferred poses are valid for all Pan joint positions, as they are only dependent on the InnerLeg and OuterLeg joints.

Combining the motion range of the three DoF Pan, InnerLeg, and OuterLeg results in various footprints that can be adopted. Figure 6 illustrates different defined stances and resulting footprint shapes for SherpaTT. The nominal height of a LEP in all stances is defined as shown in Figure 5(c) for the preferred poses. All illustrated stance examples are possible with different distances of the LEP from the origin of the respective leg’s coordinate system. If not otherwise stated, a footprint shape is generally used in the preferred PoseA.

The chosen kinematic design has the following key-features:

- Linear actuators are placed in a way that the loads and moving-distances are almost equal for both actuators, so the same parts can be used for fabrication.
- All linear actuators experience a pull-force with the robot on ground, which leads to less slackness and simplified design of the actuator’s bearings.
- High maneuverability: the rover can shift its body parallel to the ground plane (x and y direction) which allows center of gravity shifts in sloping terrain and facilitates easier pick-up and more precise deployment of a payload as for example a BaseCamp compared to moving the body in small increments by driving motions.
- The rover’s body can be rolled and pitched w.r.t. the ground and execute yaw movements, further facilitating the pick-up of payloads with the body’s EMI
- Providing a knee like structure significantly reduces the stow volume of the robot, due to the possibility of compact folding.
- Pure vertical movement of a wheel is possible, hence no change of the footprint, when the rover’s body is lifted or the wheels are adapted to sloping terrain.

Surely this kinematic setup also has drawbacks, one being a complex design process. Furthermore the torque that can be introduced to the Pan joints when the rover

is moving in slopes can cause high structural loads in the whole leg. The knee and the additional actuator introduce moving parts and bearings that are subject to those structural loads.

## 4.2 Actuators for the Suspension System

All actuators employed for the suspension system are based on the design presented in (Bartsch et al., 2016). Each actuator consists of three main parts: A gear stage on the drive side, a motor, and a stack of three printed circuit boards for local joint control. Depending on the location of the actuator in the leg, different combinations of motors and gears are used, while the control electronics are identical for all actuator types.

The Pan actuator has to provide the highest torque of all suspension actuators. To estimate the required torque, a worst case scenario was used. From the initial dimensions in the design process, a radius of  $\tilde{r}_{Pan} = 1\text{ m}$  was taken as maximum lever to generate a torque from the forces acting on the wheel<sup>2</sup>. Furthermore, a slope of  $\psi_s = 40^\circ$  with the rover’s body being parallel to the slope was assumed, and a rover mass of  $m_g = 150\text{ kg}$  was estimated during the design phase<sup>3</sup>. This results in a force  $F_{s,wc}$  for the worst case along the slope:

$$F_{s,wc} = m_g \cdot g \cdot \sin(\psi_s) \approx 946\text{ N} \quad (1)$$

As a safety margin, only two legs were considered to be bearing the full load. Using the radius  $\tilde{r}_{Pan}$ , the worst case torque a pan joint actuator has to bear was estimated as  $T_{Pan,wc}$ :

$$T_{Pan,wc} = \frac{1}{2} \cdot F_{s,wc} \cdot \tilde{r}_{Pan} = 473\text{ Nm} \quad (2)$$

As shown in Table 2, the employed gear combination is limited to a repeatable peak torque of 433 Nm, and an allowable momentary peak torque of 841 Nm according to the manufacturer’s specification. Theoretically, the chosen motor-gear combination can provide more than 2200 Nm. Since a worst case scenario with only two wheels was assumed, and the calculation done with a slope beyond the systems’s specification, the chosen combination was considered to be suitable for the system. This assumption was confirmed in all use-cases so far for the physical system. The actuators did not stall in any scenario as for example moving the legs for footprint changes in natural terrain or slope climbing with impulses and oscillations resulting from slip in steep slopes.

Similar scenarios were considered for the dimensioning of all actuators in the suspension system. A spindle drive mechanism driven by a rotational actuator is used for the linear drives for InnerLeg and OuterLeg joints. For ease of fabrication, integration and control, both

<sup>2</sup>In the final design, the preferred PoseA has a lever of  $r_{Pan} = 0.88\text{ m}$ , a fully stretched leg in kinematic singularity has a length of  $r_{Pan,max} = 1.08\text{ m}$

<sup>3</sup>Final mass  $m_g = 166\text{ kg}$ , c.f. Table 1

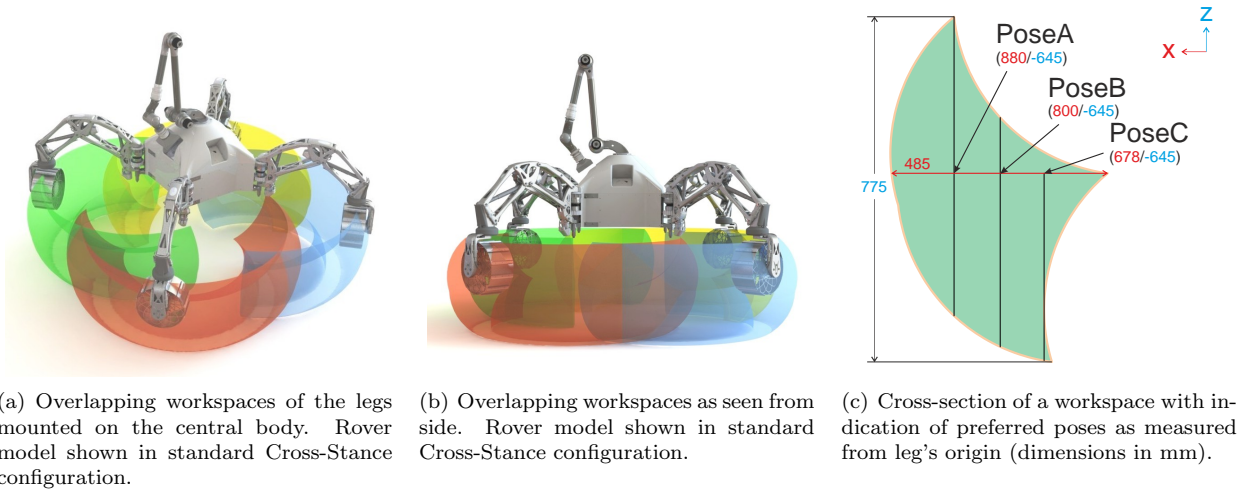


Figure 5: Workspace of the suspension system

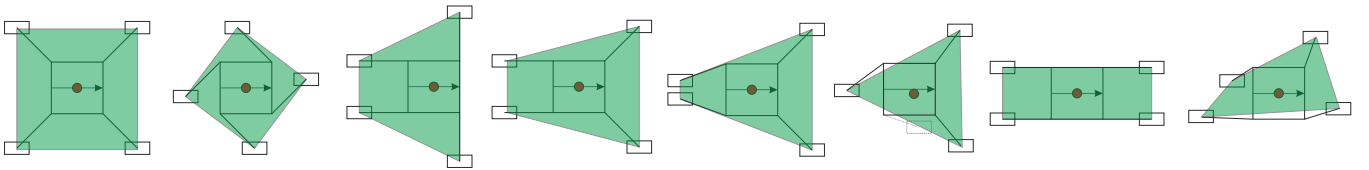


Figure 6: An extract of possible foot print configurations and resulting support polygons. From left to right: Cross-Stance, P90 (Pan joints at  $\alpha_i = 90^\circ$ ), Turtle-Front, Y-Shape, Quasi-Tripod, Tripod (one wheel disabled), Long-Stance, and arbitrary or asymmetric foot print.

linear drives of a leg are using the same hardware. For dimensioning the WheelSteering and WheelDrive actuator the aspired wheel dimensions are used together with worst case loads to estimate the required torques. The final actuator dimensioning is listed in Table 2.

### 4.3 Manipulator Arm and Body Concept

For completeness, this section briefly gives a description of the central body and the manipulation arm. The arm is not used for the experiments described in this article, details on the manipulator arm design are described in (Dettmann et al., 2011) and (Manz et al., 2012).

The manipulator arm is the hardware taken from the predecessor Sherpa. For SherpaTT the EMI is updated to the new design as presented in (Wenzel et al., 2015) and the first joint is exchanged for the same type of double stage gear actuator as used for the leg's Pan joints.

The arm is mounted centrally on the body of the rover, to be able to reach the ground all around the system. Mounted around the central manipulation tower are four EMIs that are used in the multi-robot scenario. For navigation, a HDL-32E rotating lidar is mounted on the arm such that the sensor rotates with the first DoF of the manipulation arm.

### 4.4 Robustness and Failure Response of an Actively Articulated Suspension System

Assuming the rover to get stuck in soft soil, several options to free the system exist. If a wheel breaks through

a crust and gets stuck in soft soil, the wheel can be lifted and placed in a different location. If required, the manipulation arm can add stability during the repositioning of the wheel, (Roehr et al., 2014). Alternatively, the footprint can be changed for stable tripod-stance if the arm support is not feasible. Generally, a maneuver to free a wheel from soft soil can be conducted in arbitrary footprint configurations. Detection of soft soil or other ground parameters might be possible using the force and torque information available at each wheel, this is, however, not implemented nor experimentally validated up to now.

When all wheels are subject to heavy slip and a wider area of soft soil is present, subsequent repositioning of all wheels is possible. This would lead to a kind of walking behavior to free the rover from very soft soil. The rover is not primarily designed for walking, yet the kinematics of the suspension system allow for implementation of motion patterns similar to walking locomotion.

The performance of a complex system as presented with the active suspension of SherpaTT can be impeded by failure of single joints. This is surely a factor of risk in a space mission, where currently no maintenance and repair is possible. However, the advanced locomotive capabilities allow to reach scientifically interesting and hard-to-access areas in the first place: Cliffs, crevasses and the top of inverted river beds promise to be spots with increased science return, for example in terms of geologic history and traces of former or actual presence of water. These areas cannot be safely reached with the currently deployed robots (Schenker et al., 2001), (Huntsberger et al., 2007), (Nesnas et al., 2012).

Table 2: DoF naming and actuator specifications for SherpaTT. Note that the range of motion of each DoF is generally not symmetric around the respective zero position. Pan joints use a double-stage gear.

Joint name	Index j	Angle identifier	Gear	Speed	Torque/Force (nominal)	DoF Range of Motion
Pan	0	$\alpha$	1:30 + 1:100	7 °/s	433 Nm <sup>*)</sup>	223°
InnerLeg	1	$\beta$	1:30 + linear TR14x4	12 mm/s	3500 N	70°
OuterLeg	2	$\gamma$	1:30 + linear TR14x4	12 mm/s	3500 N	81°
WheelSteering	3	$\varphi$	1:120	175 °/s	60 Nm	340°
WheelDrive	4	$\omega$	1:100	210 °/s	74 Nm	inf.

<sup>\*)</sup> theoretically the motor gear combination provides more than 2200 Nm; 433 Nm is the repeated torque rating of the gear box. A momentary peak torque of 841 Nm is rated for the gear box.

Analysing the individual joints in each of SherpaTT’s legs, the Pan joint is the least critical joint for failure: A Pan joint not able to move anymore results in less flexibility in the choice of footprints and can impede the roll-pitch adaption capabilities. General driving capabilities and ground adaption control are not affected: Force leveling control, which is the main ground adaption process (see next section), would not be affected from a failure of the Pan joints.

When InnerLeg or OuterLeg actuators fail, a rudimentary ground adaption would still be possible with all legs: Loading and unloading of the wheel is possible, however, for adaption, the wheel moves relative to the body, possibly resulting in undesirable slip or shear of the wheel on the ground. Generally, this would be counteracted by correct wheel orientation, as presented in Section 5.3; the approach is working independently from failure of individual joints and can be used without changes.

Failure of WheelSteering and WheelDrive joints results in the same problems that a passive suspension system would experience. However, the active suspension can be used to permanently remove a wheel from ground contact and drive on in a three wheel configuration as described above. If a failed WheelDrive does not block the wheel, the three remaining wheels provide enough thrust for the robot to move, the locomotion capabilities are only affected marginally. The maximum manageable slope inclines would be reduced in this case. Locomotion of SherpaTT on four wheels with only three of them powered has already been tested successfully in a qualitative experiment setting in flat outdoor terrain .

With the four wheeled-legs the loss of one leg can be generally compensated, assuming that it can at least be moved up high enough to not be in ground contact any more. This requires at least the InnerLeg or OuterLeg joint to be still functional. The remaining three wheeled-legs are then oriented in a tripod stance that distributes the wheels on a circumference around the robot’s center. The distribution is chosen such that the disabled leg’s weight is shared from the two adjacent legs. Calculation of reference forces is actually simplified with only three contact points, however, arbitrary changes in footprints are not possible anymore and roll-pitch control might also be impeded.

## 5 Control System Design

The rover’s autonomy and locomotion control are running in the Rock framework. Three basic software layers can be identified in the robot control stack:

1. *High Level, running on On-Board Computer (OBC):* Autonomous navigation and control
2. *Middle Ware, running on OBC:* Motion control, responsible for suspension articulation
3. *Low Level, running on FPGA and microcontrollers:* Joint control and sensor pre-processing

Both, high level and middle ware are implemented using the Rock framework. The system can be used with autonomous components for navigation, mapping and exploration of unknown terrain by using the highest software level. However, by only running the levels 2 and 3, direct remote operation of the system is possible by a human operator. Direct (tele-)operation and autonomous behaviors both use the same software interfaces on level 2.

This paper focusses on the experimental validation of the rover’s level 2, the *Motion Control System (MCS)*, hence the following sections focus on describing the middle ware layer. Special focus is given on the active *Ground Adaption Process (GAP)* and its submodules enabling the locomotion of the system on a natural terrain. The GAP is the software module responsible for generating LEP offsets from force measurements and body roll-pitch data in order to adapt the suspension system to the current terrain conditions.

### 5.1 Motion Control System Overview

Figure 7 provides an overview on the general structure of the MCS for SherpaTT. The three main command input types are used for human operator control or autonomous control. The commands are defined as follows:

*Definition 5.1: Motion Command 3D (MC3D).*

The three dimensional command vector  $\dot{\xi} = (\dot{x} \ \dot{y} \ \dot{\Theta})^T$  is used to command forward ( $\dot{x}$ ), lateral ( $\dot{y}$ ) and rotational ( $\dot{\Theta}$ ) velocity of the rover. All three components are independent of each other.

*Definition 5.2: BodyPosture.*

A six dimensional vector  $\mathbf{b} = (x_b, y_b, z_b, \Omega, \Phi, \Psi)^T$  containing lean values of the body within the support polygon (lean values of the body within the support polygon  $(x_b, y_b)$ , the body height  $(z_b)$  and roll  $(\Omega)$ , pitch  $(\Phi)$  and yaw  $(\Psi)$  commands of the body.

*Definition 5.3: FootPrint.*

Four three dimensional vectors  $\mathbf{g}_i = (r_i, \alpha_i, z_i)^T$  ( $i = \{0 \dots 3\}$ ) define the foot print of the robot in cylindrical coordinates (origin is the leg coordinate system, see below). This command is mainly used to alter the support polygon of the robot in the projected plane beneath the robot by changing the  $r$ - and  $\alpha$ -coordinates of each LEP. In addition to the body-height command, the  $z$ -coordinate of each LEP might be commanded individually. Figure 6 illustrates several possible foot prints resulting in different support polygons for the robot.

Internally all commands are processed such that a consistent locomotion of the system is possible. The *Drive-Mode* module handles the MC3D to orient the wheels according to the current velocity command for the rover. Additionally, the module integrates possible motions of the suspension's legs, i.e. resulting from foot print changes, to avoid internal stress that would result in slippage of the wheels. Hence, foot print changes and body posture changes can be conducted while driving, a system stop for reorganizing the suspension system is in general not required, see also Section 5.3.

BodyPosture and FootPrint commands are merged within the *LEP Command Generator* module to a single LEP-Command  $\mathbf{p}_{ref,i}$  for each leg  $i$ . The resulting command is forwarded to the *LEP Interpolator* module. The interpolator generates smooth trajectories between actual and commanded LEP, the final LEP commands  $\mathbf{p}_{ref,i}$  are written to an inverse kinematics module. The inverse kinematics module calculates the joint commands  $\mathbf{q}_{ref,i} = (\alpha_{ref,i}, \beta_{ref,i}, \gamma_{ref,i}, \varphi_{ref,i}, \omega_{ref,i})^T$  for each leg  $i$  of the suspension system.

The central GAP takes the merged LEP commands from the command generator as reference input and uses sensor data as to generate LEP output commands modifications (i.e. offsets)  $\mathbf{o}_i$ . The offsets are depending on the control modules and current ground adaption strategy. These offset values are written to the interpolated LEP commands.

In the rover's motion control system a *Ground Plane Estimator* is implemented. The ground plane is estimated by fitting a plane in a least square approach through all LEPs of wheels with ground contact. If there are only two wheels with ground contact – which can happen for short periods of time due to the width of the wheels – the plane calculation is considered not valid and the last valid plane is assumed. The fitted plane is corrected by the measured roll and pitch of the body in order to achieve a representation in a fixed coordinate frame. This module is currently not used for autonomous ground adaption, however, an experimental validation was conducted during the field tests as presented in Section 6.

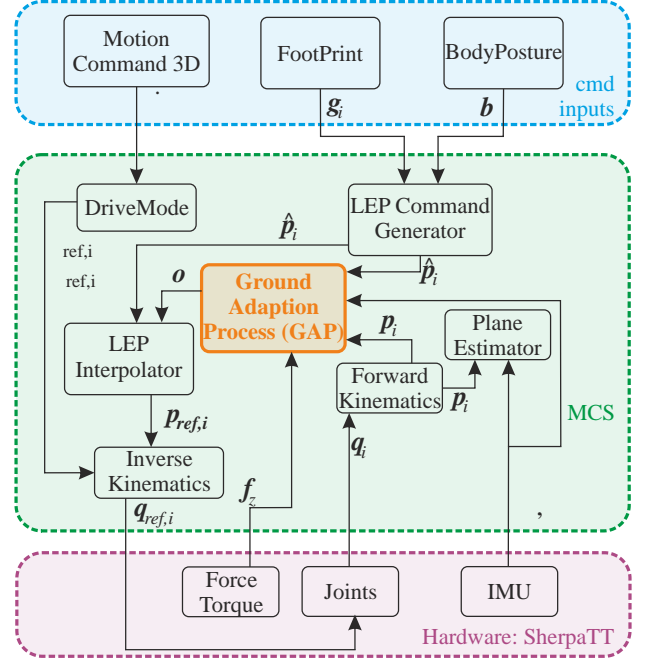


Figure 7: Simplified control structure of SherpaTT's Motion Control System (MCS) with inputs from high-level or human operator, sensor inputs and outputs to the hardware. The central Ground Adaption Process (GAP) is responsible for active terrain adaption.

## 5.2 Coordinate Systems for Locomotion Control

For locomotion control, different coordinate systems are used for ease of description and implementation of locomotion behaviors. All employed coordinate systems are right-handed.

Figure 8 illustrates the locomotion coordinate systems. The depicted coordinate systems are:

*Definition 5.4: Body Coordinate System (BCS).*

All commands for the leg end points are internally represented in this coordinate frame. Its origin is located in the center of the robot's body,  $x$  pointing forward,  $z$  pointing up, Figure 8(a).

*Definition 5.5: Shadow Coordinate System (SCS).*

At startup of the MCS, shadow coordinate system and body coordinate system BCS are identical. Body posture commands  $\mathbf{b}$  are describing the movement of the body from this initial position. Motion commands  $\xi$  are interpreted in this frame.

*Definition 5.6: Leg Coordinate System (LCS).*

Used for intuitive description of a foot print. Cylindrical coordinates are used in this frame for describing each LEP:  $\mathbf{g}_i = (r_i, \alpha, z_i)^T$ .

*Definition 5.7: Wheel Coordinate System (WCS).*

Used internally for accumulating all movements due to motion command and footprint changes. Wheel orientation and velocity are calculated in this frame.

Figure 8(b) illustrates the advantage of using a shadow coordinate system: With unchanged body posture ( $\mathbf{b} = \mathbf{0}$ ), LEP commands are the same in body coordinates

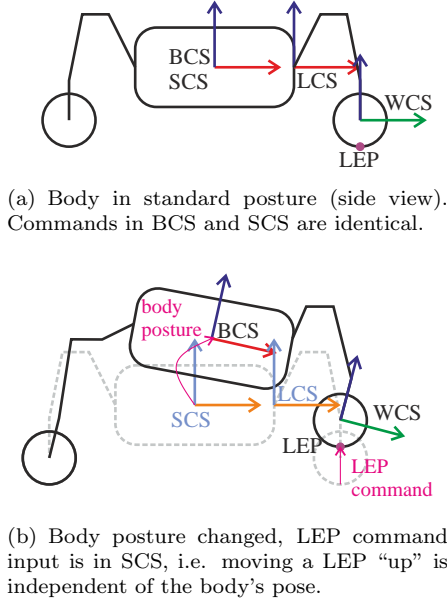


Figure 8: Important coordinate systems: Body Coordinate System BCS, Shadow Coordinate System SCS, Leg Coordinate System LCS, and Wheel Coordinate System WCS.

and in shadow coordinates. In the example illustration, a body height change together with a positive body pitch is commanded. If the odometry be described in body coordinates, movement would no longer be only in x-direction but also in z-direction. Using shadow coordinates, a forward-velocity command does not need to incorporate the body’s actual orientation. Considering the LEP control, a change in the LEP’s z-component is always perpendicular to the ground, since the leg coordinate system is also a shadow coordinate system.

### 5.3 Commanding a Rover with a Variable Footprint

Moving a rover with adaptive suspension that allows changing footprints and thus changing the location of the wheels w.r.t. the body requires some consideration of the orientation control of the wheels for locomotion. Incorrect orientation of wheels results in structural stress, undesired forces, possible slip and might lead to failure following trajectories which in turn can cause hazards for system stability and integrity.

With fixed wheel positions and assuming motion on a flat plane, all wheels need to be oriented such that all wheel axes intersect at a common point, which is the Instantaneous Center of Rotation (ICR). An ICR in infinity of the y-axis of the SCS corresponds to a pure forward movement, while positioning the ICR at the origin of the SCS results in a pure point turn of the robot<sup>4</sup>. In (Cordes et al., 2011) an explicit calculation of the wheel orientation and wheel velocity for a rover with variable footprint is presented for the sys-

tem Sherpa. The calculation assumes quasi static states and neglects the current movement of the suspension system. For SherpaTT the rover’s current velocity resulting from the commanded vector  $\xi^{SCS}$  is transformed to the frame of each wheel  $i$  to form the vector  $\xi_i^{WCS}$  of velocities at each wheel resulting from the MC3D according to Eqn. (3), where  $\mathbf{T}_{WCS,i}^{SCS}$  is the instantaneous homogeneous transformation matrix between SCS and  $WCS_i$ , which is dependent on the current pose of leg  $i$ .

$$\dot{\xi}_i^{WCS} = \mathbf{T}_{WCS,i}^{SCS} \dot{\xi}^{SCS} \quad i \in \{0, 1, 2, 3\} \quad (3)$$

The velocity of an LEP resulting from the movement of the respective suspension leg  $i$  is described as  $\dot{\lambda}_i$  and calculated using the measured angular velocities of each DoF. The combined velocity  $\dot{\mathbf{p}}$  at each LEP resulting from both, leg movement and robot movement is then calculated as

$$\dot{\mathbf{p}}_i = \dot{\xi}_i^{WCS} + \dot{\lambda}_i. \quad (4)$$

The condition for slip free motion with intersection of the wheel axes in the ICR holds only for fixed LEP positions. Introducing the component  $\dot{\lambda}_i$  in  $\dot{\mathbf{p}}$  resulting from a leg’s motion renders the condition invalid. Figure 9(a) shows the velocity vector  $\dot{\xi}^{WCS}$  at a wheel due to the rover’s motion as well as a velocity vector  $\dot{\lambda}$  of the respective leg’s motion and the combination  $\dot{\mathbf{p}}$  of both velocities for wheel alignment.

The orientation  $\varphi_i$  and velocity  $\omega_i$  of wheel  $i$  are based on  $\dot{\mathbf{p}}$  and can be calculated by

$$\varphi_i = \arctan2(\dot{p}_{i,x}, \dot{p}_{i,y}) \quad (5)$$

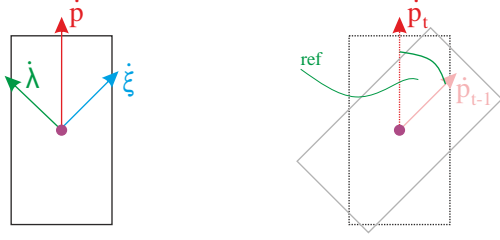
$$\omega_i = \frac{|\dot{\mathbf{p}}_i|}{r_w} \quad r_w: \text{wheel radius} \quad (6)$$

In general, two orientations of  $\varphi$  are possible for correct movement. For locomotion control in SherpaTT the solution with smaller difference to the current orientation is preferred, minimizing the movement needed in the joint to reach the desired configuration. Depending on the chosen orientation  $\varphi_i$ , the calculated wheel velocity  $\omega_i$  might need to be inverted.

With smooth trajectories, only small changes in the commanded velocity for the rover occur, resulting in incremental changes of the wheels’ steering angles. However, jumps in the reference angles  $\varphi_{ref,i}$  might occur, for example, when a FootPrint change is commanded during drive and a sudden non-zero value for  $\dot{\lambda}$  is measured.

Figure 9(b) illustrates the change of direction when a leg movement is introduced between time step  $t - 1$  and  $t$ . The difference between current and last reference steering angle is  $\Delta\varphi_{ref}$ . Since the physical WheelSteering actuator cannot change its position instantaneously to the new slip-free orientation, the whole robot has to switch into a so called re-alignment state where the

<sup>4</sup>The parallel wheel axes then are defined to intersect in infinity.



(a) Velocity combination in wheel frame.  $\dot{\mathbf{p}}$  is pointing in y-direction of WCS. (b) Velocity direction changes result in changes of the steering angle  $\varphi$ . A sudden change results in a large  $\Delta\varphi$  which cannot be followed instantaneously by the actuator.

Figure 9: Velocity components at a leg's LEP and sudden velocity direction change.

current reference values of all joints are stored and all movements are stopped until the desired wheel orientation is reached. Since in stopped state both,  $\dot{\lambda} = \mathbf{0}$  and  $\dot{\xi}^{WCS} = \mathbf{0}$ , a fading between the stored non-zero reference velocities and the actual velocities is done until the robot regains its speed, to avoid excessive WheelSteering reference angle switching.

## 5.4 Ground Adaption Process

This section describes the Ground Adaption Process (GAP) by detailing the single subcomponents and how the components interact with each other to achieve a consistent active ground adaption of the system. Generally, each of the subcomponents described in the following sections generates an LEP offset value that is added to the LEP command before passing the modified LEP command to the inverse kinematics module.

Figure 10 illustrates the structure of the GAP. The modules described in the following paragraphs are highlighted in the blue boxes. *Force Leveling Control (FLC)* and *Roll and Pitch Adaption (RPA)* are running in parallel and are writing offsets to the LEP commands. The *Active Wheel Steering Support* module is acting as an input to the Force Leveling Control by generating new reference forces in case of a stuck WheelSteering joint. After adding the LEP command and all submodules' offsets the new command is passed to the *Body Height Control* module to shift all LEPs such that the available workspace is maximized by keeping the FLC and RPA objectives, the latter prohibiting the control case shown in Figure 12(c).

### 5.4.1 Force Leveling Control Module

An important role for SherpaTT's active ground adaption is taken by the FLC component. For each wheel a contact force can be expected that is related to the position of the wheel w.r.t. the body. Using the FLC module, the expected force for each wheel is maintained, deviations due to sloping terrain are corrected and the ground contact of all wheels is ensured.

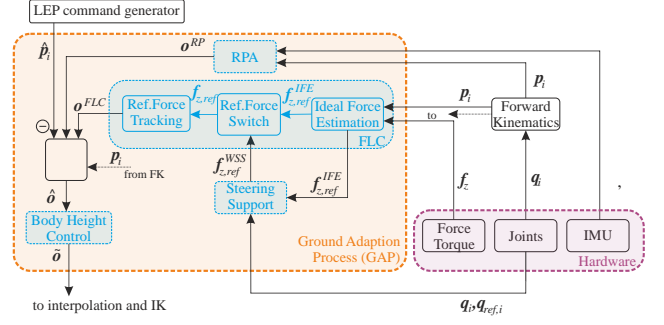


Figure 10: Structure of GAP and connection of components.

Inputs for the FLC component are the measured forces at each wheel, the location of the Center of Gravity (CoG) as well as the current coordinates of each wheel's LEP. Note that the task of FLC is to maintain the *expected* forces derived from the current foot print configuration of the robot. Improving the force distribution for locomotion, i.e. by shifting the robot's body forward when driving upslope is not the task of the FLC. The reference force switch displayed in Figure 10 is used to forward the modified reference forces as final input  $\mathbf{f}_{z,ref}$  to the force tracking in case a wheel steering support is active (see Section 5.4.2).

For each wheel  $i$  the ideal contact force  $f_{z,ref,i}$  is estimated in terms of the current footprint under the assumption of static equilibrium with only the gravitational forces and their reaction forces from the ground acting on the robot. Three constraint equations with four unknowns can be established, the resulting underdetermined system is solved using a Moore-Penrose pseudoinverse. The output of the FLC are offsets for the z-coordinates of the LEPs in order to increase or decrease the force acting on a wheel.

To generate the reference forces, the LEPs and the CoG of the robot are projected onto a gravity perpendicular 2D plane using the Inertial Measurement Unit (IMU) measurements, resulting in the 2D position of the LEPs  $(x_i \ y_i)^T$  and the 2D position of the CoG  $(x_c \ y_c)^T$ . A vector  $\mathbf{t} = (0 \ 0 \ mg)^T$  is constructed containing zero-moments around x and y axis and gravitational force with  $m$  the mass of the robot and  $g$  the acceleration due to gravity. The vector of expected reaction forces at each LEP is the vector of reference forces  $\mathbf{f}_{z,ref} = (f_{z,ref,0} \ f_{z,ref,1} \ f_{z,ref,2} \ f_{z,ref,3})^T$ . Equation (7) shows the underdetermined equation system.

$$\mathbf{A} \cdot \mathbf{f}_{z,ref} = \mathbf{t} \quad (7)$$

The matrix  $\mathbf{A}$  is defined as provided in Equation (8).

$$\mathbf{A} = \begin{pmatrix} x_0 - x_c & x_1 - x_c & x_2 - x_c & x_3 - x_c \\ y_0 - y_c & y_1 - y_c & y_2 - y_c & y_3 - y_c \\ 1 & 1 & 1 & 1 \end{pmatrix} \quad (8)$$

Constructing the Moore-Penrose pseudoinverse  $\mathbf{A}^+ = \mathbf{A}^T \cdot (\mathbf{A} \cdot \mathbf{A}^T)^{-1}$  allows to calculate  $\mathbf{f}_{z,ref}$  according to

Equation (9).

$$\mathbf{f}_{z,ref} = \mathbf{A}^+ \cdot \mathbf{t} \quad (9)$$

In each time step of MCS execution,  $\mathbf{f}_{z,ref}$  is recalculated, updating the reference values according to the current footprint and CoG location within the support polygon.

Without active leg end point control ground contact loss of one wheel can occur even in slightly irregular terrain, as there are more than three wheels on the rover that generally make ground contact. In its preferred posture the rover has a square shaped support polygon. When one of the wheels loses ground contact, the two neighbouring wheels share the main load of the system and form what is defined as *strong contact pair*. As with a rocking table the other two wheels of the *weak contact pair* tend to change their ground contact state. The two diagonals  $a_0$  (between front left and rear right) and  $a_1$  (between front right and rear left) of the support polygon are defined as *strong axis* and *weak axis* depending on the ground contact state of the wheels, (Cordes et al., 2017).

Since the strong axis has always a higher contact force than required and the weak axis always has a lower force than required, a simplified control can be used to (i) increase the speed of adaption since one pair is moving up and the other pair is moving down the same amount, (ii) reduce the number of independent controllers from four to one, and (iii) reduce interferences in force controllers of one wheel to all other wheels, since unloading one wheel results in increased load of three other wheels.

Note that the whole approach is reactive; no models of terrain-ground interaction, digital elevation maps or planning algorithms are required. This approach is chosen deliberately to keep the processing efforts as low as possible and to be able to deploy the control system on lower performance hardware in the future. Generally, reactive controllers have a better chance of being deployed successfully on space hardware with limited performance (Mumm et al., 2004). The experiments described in Section 6.4 are conducted to characterize the validity of this approach for other than the nominal Cross-Stance foot print.

### 5.4.2 Active Wheel Steering Support

Generally, the bigger the contact area of a wheel with the ground the better the traction of the wheel. However, with the steering axis above the wheel center, a bigger contact area requires a higher steering torque and also causes higher stresses in the wheel structure when steering against the ground resistance. With the possibility to lift single wheels off the ground comes the opportunity to actively unload wheels for steering support. This can be used in situations where the wheels get stuck between rocks or are subject to heavy sinkage in soft soil. Furthermore, the strength of the actuators for steering the wheel can be smaller as the actuator

does not have to be designed for worst case scenarios.

SherpaTT's MCS has a trigger for active wheel steering support which is based on the difference of actual steering angle  $\varphi_i$  and the commanded reference value  $\bar{\varphi}_i$ . The steering joints are limited conservatively in the drawable current (hence a torque limit is established) to limit mechanical loads introduced through the wheel during a steering manoeuvre. Thus when the required torque is bigger than the threshold, actual angle and reference angle for the steering DoF diverge as the wheel cannot be turned against the resistance.

Unlike most of the GAP subcomponents which are generating LEP offsets, the wheel steering support module manipulates the reference forces  $\mathbf{f}_{z,ref}$  of each wheel for unloading the wheel being stuck. In case the steering support is triggered for wheel  $j$ , the reference ground contact force  $f_{z,ref,j}$  is reduced (see also Section 5.4.1) by shifting a part  $k$  of the ground contact force to the remaining three wheels. During a wheel steering support event, the modified reference forces are used in the FLC component, once the wheel orientation reached the reference angle, the regular ground contact reference forces  $\mathbf{f}_{z,ref}^{IFE}$  from the *Ideal Force Estimation* module are used for each wheel. The value  $k$  is chosen such that the stuck wheel becomes part of the *weak contact pair*.

### 5.4.3 Roll-Pitch Adaption Module

The Roll and Pitch Adaption (RPA)-module is responsible for controlling the body's roll and pitch angles. Both, roll and pitch angle are measured with respect to gravity. To calculate an offset  $o_i^{RP}$  for each LEP, measured and commanded roll and pitch angles are compared in angle-axis form  $\{\mathbf{e}, \theta_e\}$ , where  $\mathbf{e}$  is the normalized rotation axis and  $\theta_e$  is the rotation error. As the yaw angle is not included in the RPA calculations,  $e_z = 0$ , hence  $\mathbf{e}$  is lying in the xy-plane. The distance  $d_i$  of an LEP from the rotation axis is a scaling factor for the offset, simply put, the further away a leg from the rotation axis, the greater the offset for the same rotational effect, which follows from the intercept theorem of geometry. The sign of  $o_i^{RP}$  (adapting up or down) is determined by the sign of  $\theta_e$  and the LEP location in the xy-plane  $\mathbf{p}_i = (x_i \ y_i \ 0)^T$  w.r.t.  $\mathbf{e}$ . Figure 11 illustrates the angle-axis representation.

$$o_i^{RP} = \pm d_i \tan \theta_e \quad (10)$$

$$d_i = \|\mathbf{e} \times \mathbf{p}_i\| \quad \text{because } \|\mathbf{e}\| = 1 \quad (11)$$

$$o_i^{RP} = \text{sgn}(\mathbf{p}_i \cdot \mathbf{n}) \|\mathbf{e} \times \mathbf{p}_i\| \tan \theta_e \quad (12)$$

Where  $\mathbf{n}$  is the normal of the plane spanned by the rotation axis  $\mathbf{e}$  and the basis vector along the robot's z-axis  $\hat{k} = (0 \ 0 \ 1)^T$ . Each leg's index is represented by  $i = \{0, 1, 2, 3\}$ .

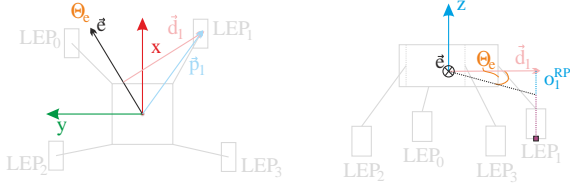


Figure 11: Illustration of angle-axis calculations for RPA-module. Left: top-view onto SCS; right: view in direction of  $\mathbf{e}$ .

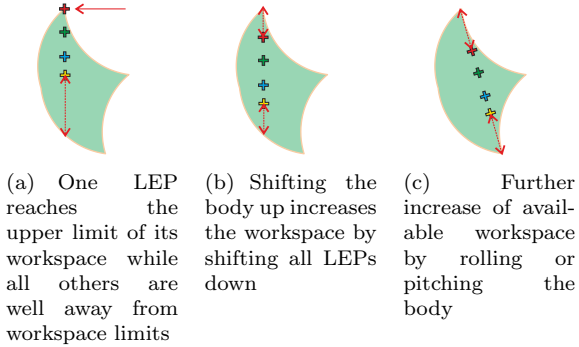


Figure 12: Body Height Control module: Shifting body to increase overall workspace of active ground adaption. This module might be not usable when specific body commands are required.

#### 5.4.4 Body Height Control Module

The Body Height Control (BHC) module is used to tailor all written offsets such that the rover's body height is altered in a way that maximizes the workspace of the legs. Figure 12(a) shows the situation, when an LEP (illustrated as red cross) reaches its upper workspace limit, rendering it impossible to further unload the wheel. In the example, all other LEPs, are still some distance from their respective limits. Hence, shifting all LEP-offsets by the same amount allows further adaption of the overall system, as shown in Figure 12(b). This effectively results in a change in body-ground clearance and hence is only possible in situations where the system is not required to keep a certain body height. A further increase of the workspace is possible by allowing the BHC module to manipulate the roll and pitch angle of the body as well, as illustrated in Figure 12(c). Again, a decision has to be made whether body roll and pitch or the quality of ground contact are of more importance in the current situation.

## 6 Experiments

This chapter describes the experiments conducted during the field trials with the rover system SherpaTT. The site for the experiments was chosen due to its reported similarity to areas on Mars (Clarke and Stoker, 2011), (Dupuis et al., 2016), (Caudill et al., 2016), (Balme et al., 2017). Preliminary indoor-experiments with SherpaTT for validation of the GAP behavior prior to the field tests are described in (Cordes et al., 2017) and (Cordes and Babu, 2016).

Experiments in three different test tracks in natural terrain were conducted during the field trip to evaluate different aspects of the rover in natural terrain. Each test track was driven in forward and backward motion, with different GAP-modes and different rover footprints. The following sections provide a description of the three terrain setups and the results from data analysis from the runs in these setups.

From the log-data of the experiments, following aspects are analysed and described in this article:

- power requirements in natural terrain, Section 6.3,
- force reference tracking and body angle control, Section 6.4,
- terrain slope estimation from proprioceptive data, Section 6.5, and
- slope climbing capabilities of SherpaTT in Section 6.6.

Summarizing the results of the following sections, it can be stated that in terms of power requirement the expectation of a general higher power draw using active suspension is confirmed. However, the extra amount of power is low compared to the overall system power requirements, at least in the presented terrain types and footprint configurations. Concerning the force reference tracking, all tested footprints showed to be usable with the force leveling methodology described in this article. The body angle control is able to keep the Root Mean Square (RMS) error below  $0.5^\circ$  in all tested terrains and footprints. In moderate slopes, the error is reduced to  $0.2^\circ$  or below. Terrain slope estimation can be confirmed to be invariant of the chosen footprint. A slight problem can be identified in the estimation when wheels loose ground contact. In terms of slope climbing experimentation, it is found that the slip in steep slopes seems to be more influenced by the chosen ground adaption mode than by the chosen footprint.

Further experimentation was conducted but is not explicitly covered in this article. This includes qualitative experiments such as successfully driving over individual high obstacles, as shown in Figure 13(a) or traversing terrain covered in small rocks of up to 100mm height with occurrence of individual larger rocks as shown in Figure 13(b). Both of these mentioned scenarios did not pose a problem for the locomotion system, however, a quantitative experimental setup was not conducted in these areas.

### 6.1 Experimental Setups

This section describes the different setups for conducting the evaluation experiments with SherpaTT. In total three test tracks, namely Flat-Terrain, Moderate-Slope, Steep-Slope are used. In each test track, single runs of the robot are conducted, while varying the driving direction (forward and backward), the footprint (two to three footprints per test track) and the GAP-mode.

The following GAP-modes are used in the experiments:



(a) Crossing a  $\approx 450$  mm high obstacle on one side of the rover



(b) Negotiating undulating terrain abundantly covered with rocks

Figure 13: SherpaTT during additional experimentation not covered in this article (Screenshots from video material)

- *noAdap* – a stiff suspension system, only the flexible metal wheels are providing adaption. This setting is chosen as a baseline to be compared with the following two other settings.
- *FLConly* – the LEP of each leg is adapted such, that the calculated reference force at the leg’s wheel is maintained
- *FLC+RPA* – force leveling control and body angle control (roll-pitch) are both active and working in parallel

Since preliminary experiments showed that using pure roll-pitch adaption without force leveling control can lead to undesired wheel-ground contact loss (Cordes et al., 2017), the GAP-mode *RPAonly* was not tested in any of the setups. The contact loss occurs for example, when a one-sided obstacle causes a pitch error of the body. To counteract the error, both front wheels are lifted up, effectively taking the wheel without obstacle off of the ground.

In each test track the footprint Cross-Stance is used. This is the nominal configuration of the rover and allows a direct comparison between the different test tracks. Additional footprints are chosen according to the rationales described in the following subsections.

### 6.1.1 Setup Flat-Terrain

Figure 14 illustrates the setup for Flat-Terrain. Main driver for this setup is baseline-data without slopes for the rover. In this setup, a straight drive for a distance of 20 m with a velocity setting of  $\dot{x} = 0.1$  m/s is commanded. The rover drives alternating forward and backward on the test track. The footprints Cross-Stance, P90, and Turtle-Front as illustrated in Table 3 are used, all with LEP in the preferred PoseA. A total of 22 runs is conducted in this setup. In this setting the ground adaption options *noAdap* and *FLConly* are used. Since there are basically no slopes in this setting, the option *FLC+RPA* was not used. Table 3 lists the conducted runs.

Table 3: Conducted runs in Flat-Terrain. Idx: Run index.

	Cross-Stance		P90		Turtle-Front	
	Amount	Idx	Amount	Idx	Amount	Idx
<i>noAdap</i>	6	1-6	4	9-12	4	17-20
<i>FLConly</i>	2	7-8	4	13-16	2	21-22
Total	8		8		6	

### 6.1.2 Setup Moderate-Slope

Figure 15 shows the general test setup of the Moderate-Slope runs. The main driver for this setup is the evaluation of the force leveling component and the combination of force leveling and roll-pitch adaption in moderate slopes.

In each run, the rover drives a 12 m traverse over the depicted natural terrain with a constant commanded velocity of  $\dot{x} = 0.1$  m/s. The track is separated into three segments of about 4 m where the first and last segment have nearly no slope, while the middle segment has a slope of approximately  $8^\circ$ . The rover drives alternatively forward and backward on the test-track, hence runs with an odd index have a negative slope, while runs with an even index are those driving upslope (rear wheels first). The front wheel pair is used to determine the traveled distance, Figure 15 shows the situation before a forward run. When stopping the rover in a forward run the rear wheels are at about the center of the third segment, this is the starting condition of the backward runs which stop in the setting as depicted in the figure.

Table 4 lists the conducted runs for this test track. A total of 30 runs is conducted in this setup, separated into the two different footprints Cross-Stance and Quasi-Tripod as illustrated in Figure 6, both with LEP in the preferred PoseA. In each footprint, runs without any active ground adaption (labeled *noAdap*), with active FLC and inactive RPA (labeled *FLConly*) and with both controllers active (labeled *FLC+RPA*) are conducted.

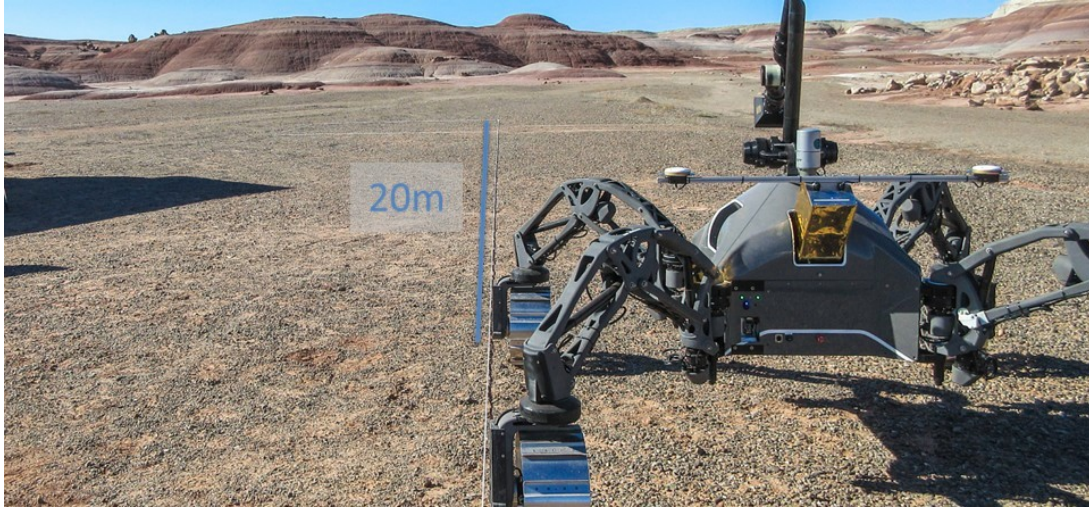


Figure 14: Experiment setup in Flat-Terrain. The DGPS module is connected to SherpaTT’s rear EMI.

Table 4: Conducted runs in Moderate-Slope.

	Cross-Stance		Quasi-Tripod	
	Amount	Idx	Amount	Idx
<i>noAdap</i>	2	1-2	2	17-18
<i>FLCOnly</i>	8	3-10	6	19-24
<i>FLC+RPA</i>	6	11-16	6	25-30
Total	16		14	

The footprint Turtle-Front from Flat-Terrain is altered to Quasi-Tripod, as the tripod configuration is especially interesting for force leveling: Using basically three contact points eliminates the undefined contact distribution and is expected to provide more stable ground contact with only the passive adaptive wheels and without active ground adaption.

### 6.1.3 Setup Steep-Slope

In this experiment series, the rover is commanded to drive on a hill with varying slope inclination of up to  $28^\circ$ . A photograph of the test slope is shown in Figure 16. For reference, 1 m long segments of the slope angle are recorded with an angle-meter. Table 5 shows the 1 m segmented slope angles on the test track.

A Differential Global Positioning System (DGPS) system is mounted on the rover for ground truth, as the main objective of this setting is the evaluation of slippage in slopes under different footprint and GAP settings. The slippage is recorded as a difference between Global Positioning System (GPS) distance and odometry distance.

The rover is commanded to drive a 17m long distance on the slope. The runs are alternating as upslope runs and downslope runs. After each run the robot was set manually to the starting position for the next run in order to compensate for slip and deviations from the track. Downhill runs start on top of the hill, uphill runs

start at the lower end of the track, with the front wheel pair as reference, hence in downslope runs (rear wheels first) the rear wheel pair is already  $\approx 2$  m into the track.

The first four (pre-test) runs were conducted with a velocity of  $0.1\text{m/s}$ , after those runs, the duricrust was broken and the system ended in 100% slippage in mid-slope for the next trials. A velocity setting of  $0.04\text{m/s}$  was then used for all remaining runs, allowing the rover to climb the slope without getting stuck in the soft soil of the broken duricrust. Nine of the runs are conducted in Cross-Stance, four runs in Y-Shape are recorded, resulting in a total of 13 valid runs on the slope.

The runs with  $0.1\text{m/s}$  are excluded from the detailed analysis in this paper. However, two successful upslope and two successful downslope runs from the pre-tests are used for comparison in the power requirement analysis in Section 6.3.

Originally, Turtle-Front was thought to be a good shape for the steep slope since the CoG of the robot is shifted to the front of the support polygon, which proved beneficial with a walking/climbing robot (Bartsch et al., 2010). However, runs in this footprint had to be aborted due to the structural loads, that were introduced to the front legs, being perpendicular to the downhill-slope force. Rotating the front leg pair into the slope results in the tested Y-Shape, which showed a higher structural stability of the rover and still has a forward shifted CoG when compared to Cross-Stance.

Further preliminary runs showed that a completely stiff suspension system (in *noAdap*-setting) poses a risk on the system stability as ground contact loss is imposing high loads to the remaining legs with ground contact and ground contact loss leads to high slip values on the remaining wheels. Even though the loads were accounted for in the mechanical design phase, the rover was not put to this risk in the field trials, hence all runs are conducted with active force leveling module in order to have all four wheels in permanent ground contact during slope drive (*FLCOnly* or *FLC+RPA* settings). Out of the 13 runs, six are conducted with active roll-pitch

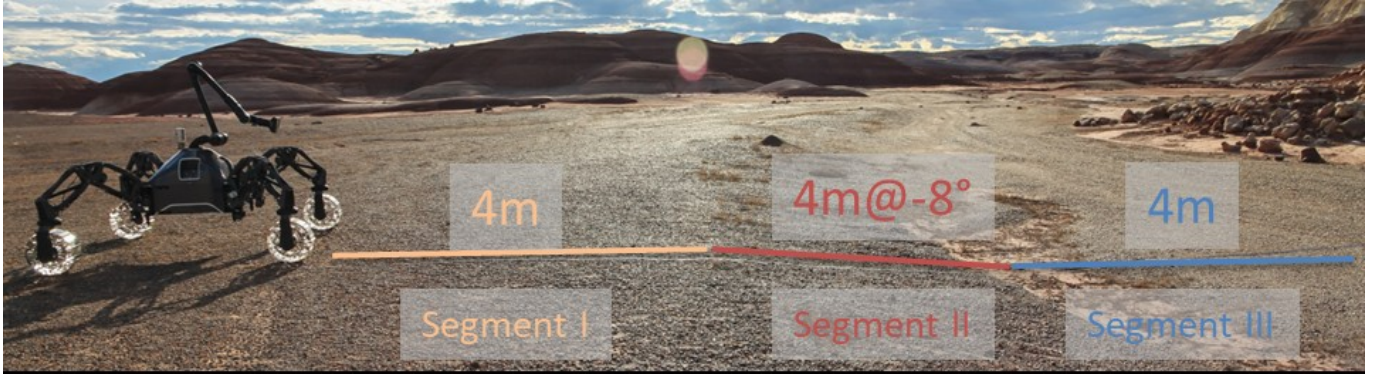


Figure 15: Experiment setup in Moderate-Slope with indicated approximate slope profile.

adaption (*FLC+RPA*). Table 6 lists the number of conducted runs and ground adaption settings.

In the steepest part of the slope, the rover reaches the workspace limit of one or more legs, even with body height correction module. In these cases, the pitch command for the rover’s body is manually altered in order to keep all LEP in the workspace for the FLC module to be able to level the forces acting on the wheels, effectively realizing a control mode as illustrated in Figure 12(c). Hence, the body angle tracking is subject to changing reference values that the rover shall maintain w.r.t. gravity.

## 6.2 Data Evaluation Methods

All evaluated data resulting from the MCS is logged at 100 Hz as this is the execution frequency of the motion control. From the data logged in the runs, most important for the following analysis are joint telemetry (current, speed, position) of all 20 DoF, force measurements at each wheel, body orientation readings from the IMU and the supply voltage of the system.

The DGPS module for ground truth in the experiments makes use of the miniature GPS aided inertial measuring system *Spacial Dual* manufactured by Advanced Communication (Advanced Navigation, 2017). With satellite based augmentation system, the horizontal position accuracy achieved is at 0.5 m, while the vertical position accuracy is at 0.8 m. The logging frequency is 20 Hz, which is the update frequency of the DGPS software module. All distances in the evaluation are calculated from latitude and longitude using python’s *geographi-clip*, and filtered with a low pass filter for noise cancellation. For synchronization with MCS-data, absolute timestamps in the log-data streams are used to match MCS and GPS data samples.

For comparison of single runs, construction of mean values, RMS error values and alike, the log data is tailored such that all data is synchronised with the beginning of the movement of the robot<sup>5</sup>. Consequently, the plots providing a distance on the x-axis are all starting with a distance of zero meters. This travelled distance on the

<sup>5</sup>The start of movement is not equidistant (time-wise) from the start of logging in all runs.

x-axis is an estimated value from the robot’s proprioceptive data, thus a slight error in synchronicity due to slip and sensor inaccuracy might be present in the data.

All experiments are conducted with the robot running on battery power. Once the primary battery is low, the system automatically switches to the (identical) secondary battery. For power calculations presented in Section 6.3, always the actual supply voltage is used. Pulse Width Modulation (PWM) duty cycle and joint currents are taken from the respective joint’s telemetry data stream.

When comparing the data of different runs, a mean value is calculated with a standard deviation around that mean value. In the plots presented in the following, a light band around each mean-plot illustrates the standard deviation of the runs. For power analysis, first a mean power draw for each single run is calculated. All runs with same settings (same footprint, GAP-mode, test track) are then used to build a mean power value for this setting.

The RMS error values of force tracking provided in the tables are generated from the means over all respective runs, resulting in a single value for comparison of the effects of footprints and active adaption modes. Based on the RMS error values, a percentual change between the runs with and without active ground adaption is calculated. Absolute errors are denoted as  $e$  with appropriate index, RMS values of errors are denoted  $\hat{e}$ , while the mean of errors over several runs is denoted as  $\bar{e}$ . General definitions of the most commonly used symbols in the following sections are provided in Table 7.

## 6.3 Power Requirements for Active Ground Adaption

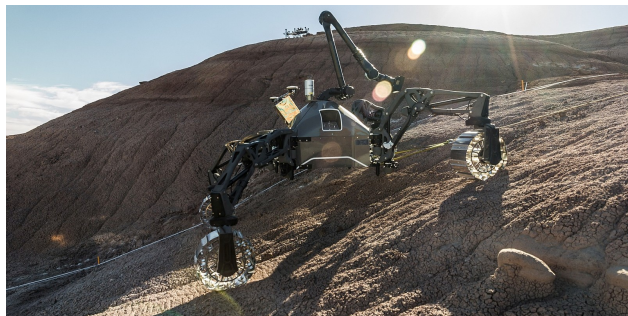
One of the main questions when analysing a rover with an active suspension is the power requirement for the active adaption to the terrain. The experiments in this section shall determine the “power overhead” for the active suspension system.

Table 5: Slope angles for Steep-Slope tests.

Segment [m]	0-1	1-2	2-3	3-4	4-5	5-6	6-7	7-8	8-9
Slope	9.5°	10°	10°	11°	15°	16°	28°	22°	25°
Segment [m]	9-10	10-11	11-12	12-13	13-14	14-15	15-16	16-17	17-18
Slope	28°	28°	20°	20°	15°	10°	10°	0°	0°



(a) Photograph of the slope with indication of test track. Length of track is 17m.



(b) SherpaTT in the steepest section of the slope with active roll-pitch adaption.

Figure 16: Experimental setup for Steep-Slope tests.

Table 6: Conducted runs in Steep-Slope.

	Cross-Stance		Y-Shape	
	Amount	Idx	Amount	Idx
<i>FLConly</i>	5	1-5	2	10-11
<i>FLC+RPA</i>	4	6-9	2	12-13
Total	9		4	

### 6.3.1 Presumption

A system with passive suspension has basically no power requirement for ground adaption, only actuators for steering and driving the wheels need to be powered. For active suspension, all actuators that are responsible for terrain adaption add to the power requirements of the system. Consequently, the analysis in this section splits SherpaTT's power for locomotion  $P_l$  into the power for the drive system  $P_d$  (all WheelSteering and WheelDrive joints) and for the suspension system  $P_s$  (all Pan, InnerLeg and OuterLeg joints).

It is expected that more power is required for the suspension with increasing terrain difficulty. Furthermore, a simple force leveling requires less movements of the suspension's actuators, when compared to force leveling and body roll-pitch control. Hence, the cases with active roll-pitch adaption are expected to consume more power.

All three settings described in Section 6.1 are used to characterize the power overhead for active adaption in SherpaTT, additionally two pre-test runs with 0.1 m/s velocity setting are analysed for better comparability with the runs in Flat-Terrain and Moderate-Slope. All power values presented are based on current measurements on joint level as well as central supply voltage measurement for the legs.

### 6.3.2 Results

In the current integration state, the base power consumption from the logic units, sensors, wireless communication, and DC/DC converters is for all runs in all settings  $P_b \approx 160 W$  when a DGPS module is connected and  $P_b \approx 150 W$  without connected DGPS module. This power is required regardless of the locomotion state of the robot.  $P_b$  is a constant power requirement and not taken into account in the following analysis, which focusses on the locomotion power requirements.

Table 8 lists the mean power values from Flat-Terrain runs. As can be expected, inactive adaption results in no power consumption from the suspension system. The total power in the runs with *noAdap* is thus equal to the power consumption from the WheelSteering and WheelDrive joints and is around 45 W to 48 W for all footprints. With active force leveling control, the rover mean power increases by 7 W - 9 W for controlling the 12 active DoF of the suspension system. The deviation for the suspension system power consumption means is below 1 W, indicating a very constant power consumption over the different runs.

For Moderate-Slope a similar behavior can be found, as provided in Table 9. In the case with *FLConly* adaption mode, 13.6 W and 11.1 W of power are required for adaption to the ground in Cross-Stance and Quasi-Tripod, respectively. When adding the roll-pitch control in *FLC+RPA* mode, the power requirement increases in both footprints. The reason for the increased power requirement is that the InnerLeg and OuterLeg actuators have to adapt more to the terrain in order to keep the body in constant orientation w.r.t. gravity. Again the standard deviation for the suspension system's power consumption is below 1 W in all shown cases.

Comparing Cross-Stance in Flat-Terrain with Moderate-Slope, an increase in power requirement  $P_l$  can be seen from flat terrain (around 54 W) to mod-

Symbol	Explanation	Symbol	Explanation
$P_b$	Basic power consumption	$P_l = P_d + P_s$	Power for locomotion
$P_d$	Power for drives	$P_s$	Power for suspension
$e_{a0}$	Force error on Axis 0 (FL/RR)	$e_{a1}$	Force error on Axis 1 (FR/RL)
$e_{fi}$	Force error at wheel $i$		
$e_r$	Roll error	$e_p$	Pitch error
$\sigma_X$	Standard deviation for $\bar{X}$		

Table 7: Main symbols for evaluation

Table 8: Mean values and standard deviation for power consumption for locomotion in Flat-Terrain. Locomotion velocity  $v = 0.1 \text{ m/s}$

	Cross-Stance <i>noAdap</i> <i>FLConly</i>		P90 <i>noAdap</i> <i>FLConly</i>		Turtle-Front <i>noAdap</i> <i>FLConly</i>	
$\bar{P}_l / \sigma_{P_l}$	44.8 W / 3.5 W	53.9 W / 4.7 W	45.1 W / 4.8 W	54.0 W / 3.3 W	48.8 W / 4.6 W	54.6 W / 5.2 W
$\bar{P}_d / \sigma_{P_d}$	44.8 W / 3.5 W	44.9 W / 4.0 W	45.1 W / 4.8 W	47.2 W / 3.5 W	48.8 W / 4.6 W	47.3 W / 5.4 W
$\bar{P}_s / \sigma_{P_s}$	0.0 W / 0.0 W	9.0 W / 0.7 W	0.0 W / 0.0 W	6.8 W / 0.4 W	0.0 W / 0.0 W	7.3 W / 0.2 W

erate slope (around 75 W “up”). The increase is mostly from the wheel drives: when comparing Cross-Stance in *FLConly* the suspension system requires a mean of 9.0 W for force control in flat terrain and 13.6 W in the moderate slope of Moderate-Slope.

In the Steep-Slope setting, the suspension system power requirement for controlling the wheel-ground contact forces is not significantly higher when compared to the other two settings.

Table 10 shows the data from Steep-Slope with velocity setting of 0.04 m/s. The upslope and downslope runs in *FLConly* mode show a mean power requirement of around 12 W for both footprints. Due to the steeper inclination the power requirement  $P_s$  for *FLC+RPA* mode is noticeably higher, as the steeper slope requires more adaption from the suspension joints, around 20 W are required in this locomotion mode. The standard deviation over the suspension power consumption means of all runs is below 1 W for all shown cases of the table.

For better comparison the power requirements from the two pre-test upslope runs (Cross-Stance, *FLConly*,  $\dot{x} = 0.1 \text{ m/s}$ ) are provided as follows: Mean total locomotion power  $\bar{P}_l = 178.3 \text{ W}$ , separated into  $\bar{P}_d = 156.8 \text{ W}$  and  $\bar{P}_s = 21.5 \text{ W}$ . Looking at the pre-test downslope runs shows that the wheels have a netto power generation of  $\bar{P}_d = -6.98 \text{ W}$ , which is due to less power required for braking the rover. Table 11 lists all mean power values for upslope runs in Cross-Stance and *FLConly* as measured in the three terrain profiles and with two velocity settings in Steep-Slope.

In the table, the mean values from Moderate-Slope are taken as baseline values, the other settings are compared against these values. absolute change and relative change w.r.t. Moderate-Slope are provided in the table. Due to the very low power consumption of the suspension system in flat terrain, the relative change of  $P_s$  in Moderate-Slope is with 51.1% higher than that of  $P_d$

(37.4%). However, in Steep-Slope with reduced velocity setting, the  $P_s$  is only 35.6% higher than in Moderate-Slope, while  $P_d$  increases by 105.1%.

The last row of Table 11 indicates the fraction of the suspension system power of the overall locomotion power. In flat terrain and moderate slopes, the share of the suspension system is at 17% and 18% of the overall locomotion power. For the Steep-Slope setting, regardless of the commanded speed, the suspension power share drops to 12%, because of the main increase in power for the drive system. The mean power values are also illustrated in Figure 17

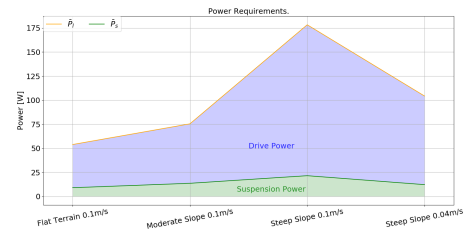


Figure 17: Power for locomotion in different terrains

The most noticeable difference in power consumption in Steep-Slope is neither the footprint nor the GAP-mode, the main difference in power consumption is between up- and downslope runs. Figure 18 shows the power mean values for each single run in Steep-Slope setup ( $\dot{x} = 0.040 \text{ m/s}$ ). A clear difference in the mean power consumption  $\bar{P}_{l,n}$  from the battery can be seen when comparing the downslope runs (odd index) with the upslope runs (even index). The mean downslope power requirement regardless of the GAP-mode is around 17 W in Cross-Stance and at  $\approx 19 \text{ W}$  for Y-Shape. Upslope power over all runs of one GAP-mode is 104 W and 118 W for Cross-Stance and 101 W and 119 W for Y-Shape.

A high standard deviation of the single-run mean values can be observed, as indicated by the black bars in the

Table 9: Mean values and standard deviation for power consumption for locomotion in Moderate-Slope. Locomotion velocity  $v = 0.1 \text{ m/s}$

Footprint	mean/dev	Up <i>noAdap</i>	Up <i>FLCOnly</i>	Up <i>FLC+RPA</i>	Dwn <i>noAdap</i>	Dwn <i>FLCOnly</i>	Dwn <i>FLC+RPA</i>
	$\bar{P}_l / \sigma_{P_l}$	64.8 W / n.a. <sup>*)</sup>	75.4 W / 1.0 W	82.3 W / 2.3 W	49.9 W / n.a. <sup>*)</sup>	58.8 W / 1.1 W	66.4 W / 2.4 W
	$\bar{P}_d / \sigma_{P_d}$	64.8 W / n.a. <sup>*)</sup>	61.7 W / 0.8 W	60.9 W / 2.1 W	49.9 W / n.a. <sup>*)</sup>	45.4 W / 0.9 W	45.0 W / 2.2 W
	$\bar{P}_s / \sigma_{P_s}$	0.0 W / n.a. <sup>*)</sup>	13.6 W / 0.7 W	21.4 W / 0.3 W	0.0 W / n.a. <sup>*)</sup>	13.4 W / 0.8 W	21.5 W / 0.2 W
	$\bar{P}_l / \sigma_{P_l}$	65.8 W / n.a. <sup>*)</sup>	72.0 W / 1.2 W	85.6 W / 2.0 W	49.0 W / n.a. <sup>*)</sup>	56.6 W / 1.3 W	68.5 W / 1.5 W
	$\bar{P}_d / \sigma_{P_d}$	65.8 W / n.a. <sup>*)</sup>	60.9 W / 1.3 W	61.9 W / 2.0 W	49.0 W / n.a. <sup>*)</sup>	45.5 W / 1.4 W	45.1 W / 1.6 W
	$\bar{P}_s / \sigma_{P_s}$	0.0 W / n.a. <sup>*)</sup>	11.1 W / 0.2 W	23.7 W / 0.0 W	0.0 W / n.a. <sup>*)</sup>	11.1 W / 0.2 W	23.4 W / 0.4 W

<sup>\*)</sup> single runs: no std-deviation values

Table 10: Mean values and standard deviation for power consumption for locomotion in runs in Steep-Slope. Values are separated for up- and downslope drives and GAP-mode. Locomotion velocity  $v = 0.040 \text{ m/s}$

Footprint	Pwr mean/dev	Up <i>FLCOnly</i>	Up <i>FLC+RPA</i>	Dwn <i>FLCOnly</i>	Dwn <i>FLC+RPA</i>
	$\bar{P}_l / \sigma_{P_l}$	104.3 W / 1.5 W	118.1 W / 6.0 W	14.5 W / 0.3 W	20.5 W / 0.5 W
	$\bar{P}_d / \sigma_{P_d}$	92.1 W / 1.4 W	95.9 W / 6.4 W	2.3 W / 0.2 W	0.5 W / 0.2 W
	$\bar{P}_s / \sigma_{P_s}$	12.2 W / 0.0 W	22.2 W / 0.3 W	12.2 W / 0.1 W	20.0 W / 0.3 W
	$\bar{P}_l / \sigma_{P_l}$	100.8 W / n.a. <sup>*)</sup>	118.7 W / n.a. <sup>*)</sup>	15.1 W / n.a. <sup>*)</sup>	22.0 W / n.a. <sup>*)</sup>
	$\bar{P}_d / \sigma_{P_d}$	89.2 W / n.a. <sup>*)</sup>	99.5 W / n.a. <sup>*)</sup>	2.7 W / n.a. <sup>*)</sup>	0.9 W / n.a. <sup>*)</sup>
	$\bar{P}_s / \sigma_{P_s}$	11.6 W / n.a. <sup>*)</sup>	19.2 W / n.a. <sup>*)</sup>	12.4 W / n.a. <sup>*)</sup>	21.2 W / n.a. <sup>*)</sup>

<sup>\*)</sup> single runs: no std-deviation values

Table 11: Example Cross-Stance, *FLCOnly*: Change of mean power consumption over terrain settings

	Flat-Terrain 0.1 m/s	Moderate-Slope 0.1 m/s			Steep-Slope 0.1 m/s			Steep-Slope 0.04 m/s		
	abs	abs	change		abs	change		abs	change	
$\bar{P}_l$	53.9 W	75.4 W	+21.5 W	+39.9 %	178.3 W	+124.4 W	+230.9 %	104.3 W	+50.4 W	+93.5 %
$\bar{P}_d$	44.9 W	61.7 W	+16.8 W	+37.4 %	156.8 W	+111.9 W	+249.3 %	92.1 W	+47.2 W	+105.1 %
$\bar{P}_s$	9.0 W	13.6 W	+4.6 W	+51.1 %	21.5 W	+12.5 W	+138.9 %	12.2 W	+3.2 W	+35.6 %
ratio $\bar{P}_s / \bar{P}_l$										
$\frac{\bar{P}_s}{\bar{P}_l}$	0.17	0.18			0.12			0.12		

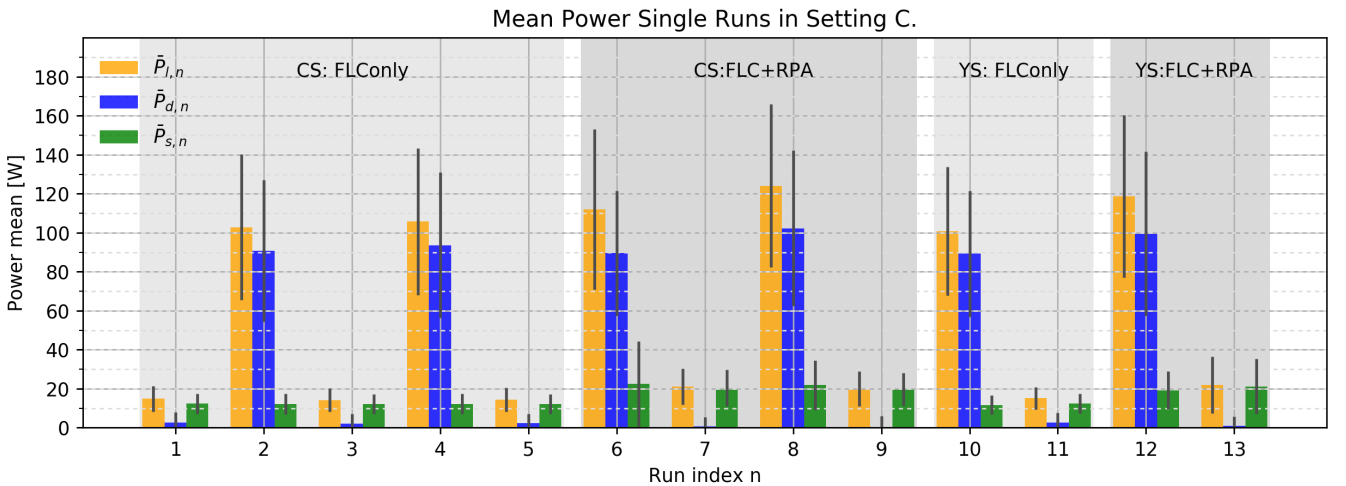


Figure 18: Individual run power consumption in Steep-Slope (mean values per run). Black error bars indicate the standard deviation for each run's mean value. CS: Cross-Stance; YS: Y-Shape.

figure. This is due to the changing power consumption during the run which starts in moderate slopes, has a peak slope in the middle of the run and a zero degree slope on top of the test hill. Figure 19 shows the mean power consumption over all runs in Steep-Slope with Cross-Stance to illustrate the power consumption over the locomotion distance in the slope.

In moderate inclinations at the begin and end of a run, only a small amount of power is required when compared to the steepest parts of the slope. Upslope it can be seen that a moderate 40 W are from the wheel's joints in the first two meters of the slope. The maximum mean value is around 11-12 m into the slope, where 160 W are required. Downslope the wheels require around 10 W in the moderate slopes at start and stop of the runs but temporarily generate power in the steeper parts.

The power for the suspension units is comparatively constant, yet there is a peak around 7.5 m visible in Figure 19(a), which results from one single run event: In Run 6 there was a heavy slip event with 100% slip in mid-run, causing the robot to shake due to the wheels' grousers until slip-value dropped below 100%. During that event, the suspension system tried to compensate the loading and unloading of the wheels, resulting in a higher power consumption from the suspension system to compensate the contact loss, Figure 20.

### 6.3.3 Conclusion: Power Analysis

With the presented experiments it is shown that the active adaption to the surface is not the main power consumer in the system SherpaTT. In fact in moderate terrain (Settings A and B), the power consumption is around 10 W for *FLCOnly* mode, while the overall power consumption in these cases is 54 W in flat terrain and around 75 W in moderate slopes. The change in power requirement is mostly due to the higher power requirements of the rover drive system, the suspension has the same power requirements in both settings. In steep slopes with *FLCOnly* the overall power requirement rises to above 100 W in upslope runs with reduced velocity, while the suspension system requires less than 12.5 W (*FLCOnly*). The fraction of power requirement of the active suspension drops from moderate terrain with about 20% to 12% in steep slopes. Thus, while enabling the rover to drive in steep terrain, the fraction of power for the suspension system in these terrains plays a smaller role in the overall power consumption of the rover.

Figure 17 shows the development of power requirement for locomotion over the three terrain settings. For Steep-Slope there are also the pre-test runs with velocity setting 0.1 m/s included in the plot. It is clearly visible that the main increase in power consumption with increasing terrain inclines is due to the drive system, hence the WheelSteering and WheelDrive actuators also present in a comparable rover with passive suspension system are the main power sinks.

The final conclusion concerning the power requirements

for active ground adaption is that there is indeed a higher power requirement than in passive suspension would be. However, the extra amount of power is low compared to the variance of power at the wheels required for different terrains. Furthermore the active suspension provides more abilities than passive suspension with active body angle control or flexible footprint configurations not being possible with a passive suspension. It can be expected, that the power requirement for the suspension increases in undulating terrain, as the legs need to move the wheels longer distances and more frequently. This needs further consideration in upcoming experiments.

## 6.4 Force Reference Tracking and Body Angle Control

The FLC module is used for permanent ground contact of each wheel. For roll and pitch adaption for the body the RPA module is used. Both modules of GAP are evaluated in this chapter.

### 6.4.1 Presumption

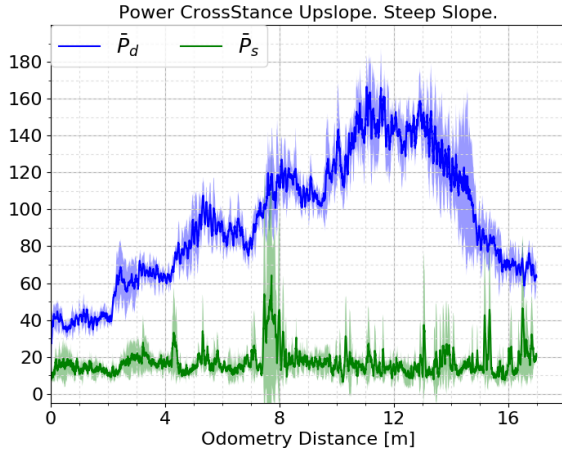
In the presented experiments the ability of the force leveling control module to cope with different footprints shall be evaluated. Since a simplified controller based on the strong and weak contact axis and combined control for two wheels is used, it is expected, that other footprints than Cross-Stance impede the capability of FLC to track the reference forces. Furthermore, the effect of different terrain inclinations on the quality of ground adaption is analysed.

The body angle control is expected to have no significant differences between the footprints as it is implemented independent of the footprint, each LEP's distance to the rotation axis is regarded separately.

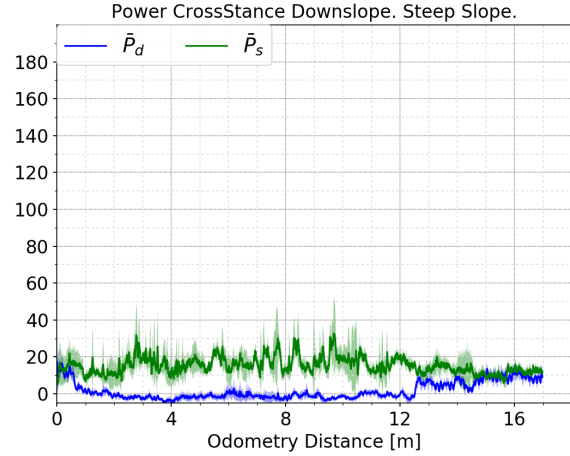
### 6.4.2 Results

All three experiment settings are used to validate the reference force tracking of the FLC component while Moderate-Slope and Steep-Slope are used to evaluate the body angle tracking of the RPA component as well. The results for the FLC component presented in this section are mainly based on the force tracking errors  $e_{a0}$  on the contact axis 0 (front left and rear right wheel). An evaluation based on one contact axis is valid, since all tested footprints have a left-right symmetry, resulting in symmetrical force errors on the two contact axes, hence  $e_{a0} = -e_{a1}$  for all runs.

Figure 21 shows the mean error plots with standard deviations for the runs from Flat-Terrain, while Table 12 lists all RMS results from this setting and indicates the changes resulting from the active adaption process with negative values indicating an improvement (reduction of the error). The errors  $\hat{e}_r$  and  $\hat{e}_p$  for body attitude control are small (mostly below  $1^\circ$ ), due to the flat terrain. Since no runs with active roll-pitch adaption are conducted in Flat-Terrain, these values are not discussed in

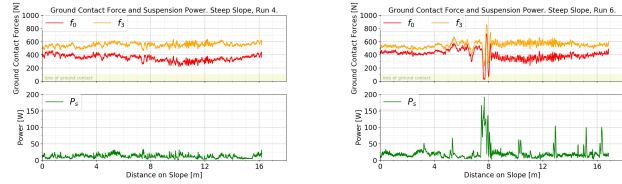


(a) Power over all upslope runs: Power  $\bar{P}_d$  increases with slope.



(b) Power over all downslope runs: Temporary power generation from wheel drives.

Figure 19: Power over up- and downslope runs in Steep-Slope. Means over all runs in Cross-Stance.



(a) Run 4 in Steep-Slope. Regular slip in slope, all wheels with permanent ground contact. Power consumption for suspension system without significant peaks.

(b) Run 6 in Steep-Slope. Heavy Slip (100%) in the middle of the slope leads to loading and unloading of the wheels. Loss of ground contact for front left wheel around 7.5 m into the slope leads to high energy consumption for the suspension system in order to get all wheels into ground contact as quick as possible.

Figure 20: Comparison of regular run and run with heavy slip: Forces FL and RR and power for suspension system.

detail.

Without active adaption, the forces deviate from the reference forces due to temporary ground contact loss and non ideal force distribution. As obvious from the plot and visible in the data in Table 12, the P90 setting has smaller force errors without active adaption in this flat ground traverse than Cross-Stance. The reason for this might be found in the smaller footprint, which reduces the tendency to tip over one of the two contact axes, this can also be seen in the smaller amount of power needed for adaption in this footprint, see Table 8.

Using the force leveling control module reduces the errors in all footprint settings. As the absolute error is already small for P90 without active adaption, the relative improvement is not that high, yet the absolute values with force leveling are comparable to those of Moderate-Slope with different footprints (see below).

All runs with active ground adaption in Cross-Stance for Flat-Terrain had a re-orientation phase of the wheels in the beginning of the run, leading to higher force er-

rors due to changing reference values. Consequently a higher RMS error value ( $\approx 56$  N compared to  $\approx 38$  N in Moderate-Slope) is observed. This is also visible in the data plot in Figure 21(b), where a peak of  $\bar{e}_{a0}$  in Cross-Stance is visible at the beginning and the end of the runs. Excluding the peaks results in  $\hat{e}_{a0}(1\text{ m} \dots 19\text{ m}) \approx 43$  N for Cross-Stance.

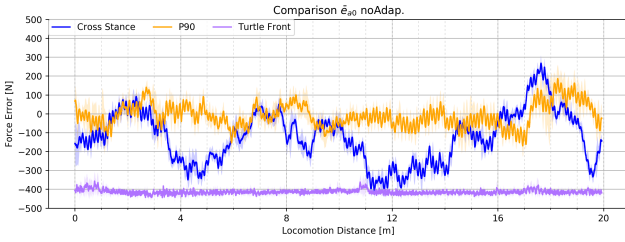
A separate analysis has to be done for the Turtle-Front runs. The plot for the runs without adaption in Figure 21(a) shows a nearly constant mean error  $\bar{e}_{a0}$ . In fact, in this footprint the rear right wheel was without ground contact most of the time in all four runs, effectively leading to a tripod configuration. This is also the reason for the seemingly great improvements in the body angle error values  $\Delta\hat{e}_r = -60\%$  and  $\Delta\hat{e}_p = -30\%$  for this footprint even without active RPA-module: All wheels had ground-contact with *FLOnly* setting, reducing the roll and pitch error even without active RPA-module. Note that the absolute values of improvement are only around  $0.4^\circ$ .

As listed in Table 3, only two runs were conducted for the active adaption case in Turtle-Front. In one of the two runs a reorientation of the wheels occurred in the first few meters of the run, explaining the higher RMS error value  $\hat{e}_{a0}$  of about 81 N. After the reorientation event the FLC module was able to reduce the force error to comparable values as in the other two footprint configurations, Figure 21(b). Using only the error values between 3 m and 19 m for RMS calculation results in a value  $\hat{e}_{a0}(3\text{ m} \dots 19\text{ m}) \approx 34$  N for Turtle-Front which is well in the range of the other footprints and the runs in Moderate-Slope. However, due to the small number of runs, the values for Turtle-Front in Table 12 cannot be taken into account of the analysis. Qualitatively the adaption seems to be able to cope with this footprint, yet a more thorough analysis is needed for a quantitative statement.

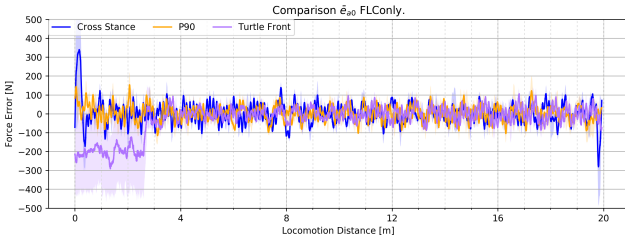
A similar result as in Flat-Terrain can be observed for Moderate-Slope. Figure 22 shows the force errors on the FL-RR contact axis for Cross-Stance and Quasi-Tripod

Table 12: RMS error values of forces, roll and pitch in Flat-Terrain. Percentual change when compared to *noAdap*. Gravitational force of rover is  $F_g \approx 1628$  N.

Footprint	GAP mode	$\hat{e}_{f0}$	$\hat{e}_{f1}$	$\hat{e}_{f2}$	$\hat{e}_{f3}$	$\hat{e}_{a0}$	$\hat{e}_{a1}$	$\hat{e}_r$	$\hat{e}_p$
	<i>noAdap</i>	123.64 N	74.36 N	117.54 N	70.77 N	183.43 N	183.43 N	0.34°	0.57°
	<i>FLConly</i>	47.77 N -61 %	45.94 N -38 %	44.32 N -62 %	49.72 N -30 %	55.96 N -69 %	55.96 N -69 %	0.36° +7 %	0.59° +3 %
	<i>noAdap</i>	35.21 N	70.70 N	79.10 N	39.47 N	61.75 N	61.75 N	0.59°	0.44°
	<i>FLConly</i>	29.74 N -16 %	76.04 N +8 %	74.65 N -6 %	28.90 N -27 %	39.64 N -36 %	39.64 N -36 %	0.64° +9 %	0.41° -6 %
	<i>noAdap</i>	126.97 N	92.32 N	322.34 N	287.64 N	414.51 N	414.51 N	0.64°	1.44°
	<i>FLConly</i>	32.28 N -75 %	21.05 N -77 %	63.54 N -80 %	58.52 N -80 %	81.43 N -80 %	81.43 N -80 %	0.25° -60 %	1.02° -30 %



(a) Comparison with no active ground adaption



(b) Comparison with *FLConly* setting

Figure 21: Force tracking errors in Flat-Terrain. Comparison of effects of GAP-modes and between three footprint configurations on FL-RR axis.

in Moderate-Slope. Table 13 lists all deviation values.

As expected, in Cross-Stance without active adaption, the force error shows high deviations from the reference values which is due to tilting over the strong contact axis, c.f. Section 5.4.1. The errors in Quasi-Tripod are smaller, as the configuration is close to a tripod which is intrinsically stable in rough terrain.

Activating the force leveling control improves the force tracking significantly: In Cross-Stance, the RMS error value  $\hat{e}_{a0}$  drops by 92%, the improvement is less significant in Quasi-Tripod (drop by 79%), which is due to the smaller error value in the case without active adaption which is used as baseline. The absolute errors, however, are in a comparable range (34.3 N in Cross-Stance and 36.7 N in Quasi-Tripod), showing the capability of the FLC component adapt the forces independently of the footprint.

Additionally activating the RPA component does not noticeably affect the force values. The force errors are in the same range, a comparison of the force-error plots in Figures 22(b) and 22(c) shows no significant difference

between the two active adaption modes.

Concerning the RMS error values  $\hat{e}_r$  and  $\hat{e}_p$  of the errors in the body's roll and pitch angle, the force leveling alone has not much effect on the body angles of the rover. The improvement of 10% for  $\hat{e}_r$  in Cross-Stance has to be considered due to the natural terrain and possible changes in the exact trajectory of the rover. Note that the absolute improvement is as small as  $0.15^\circ$ . The RPA component, however, improves the attitude control of the rover's body by as much as 97% without a significant effect on the FLC component. From the absolute values, it can be observed that the roll adaption in Quasi-Tripod seems to be slightly less accurate while the pitch correction reduces the errors for both footprints to  $0.1^\circ$  and  $0.12^\circ$ .

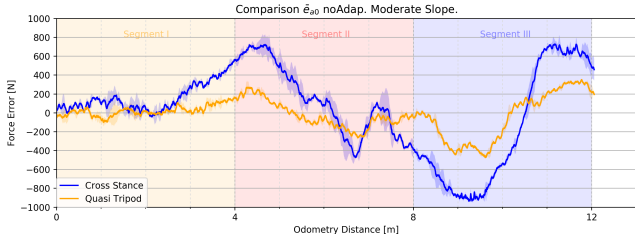
In Steep-Slope, higher slippage of the robot is present due to the slope the robot is driving on. The different slippage events over the individual runs do not allow to build means over all runs as done for analysis of runs in settings Flat-Terrain and Moderate-Slope. Hence, an evaluation interpreting the data of the separate runs is necessary for Steep-Slope. Figure 23 shows the RMS error values  $\hat{e}_{a0}$ ,  $\hat{e}_r$ ,  $\hat{e}_p$  for all single runs in Steep-Slope, Table 14 lists the values and additionally the values for single legs  $\hat{e}_{fi}$  and force axis 1,  $\hat{e}_{a1}$ .

All  $\hat{e}_{a0}$  values, except for Run 6, are in the same range regardless of the footprint or active or inactive roll-pitch adaption. Furthermore, the values are in the same range of  $\hat{e}_{a0}$  in Cross-Stance with *FLConly* in Flat-Terrain. The slip event in Run 6 (see also Section 6.3), caused loading/unloading of the wheels, hence higher force tracking errors occurred which are visible in the RMS value of this run. Figures 20 and 26 show the forces  $f_0$  and  $f_3$  during that run, the unloading down to ground contact loss ( $f_0 < 100$  N) is visible starting from about 7.5 m into the slope.

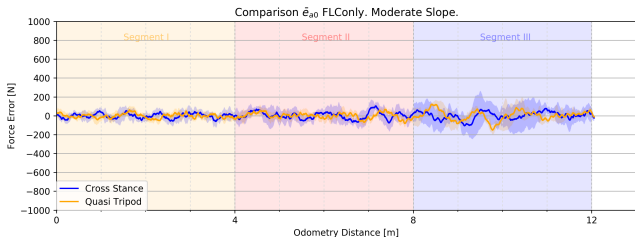
As can be expected, without roll-pitch adaption, the body angles are basically following the slope the robot is driving on, hence the comparatively huge errors in pitch (rover is driving up/down slope) and moderate roll angles in *FLConly* mode. The relatively high scattering of the RMS pitch error with max  $21^\circ$  in Run 11 and min  $15.1^\circ$  in Run 5 can be explained by the rough natural terrain which caused the rover to change its ori-

Table 13: RMS error values of forces, roll and pitch in Moderate-Slope. Percentual change when compared to *noAdap*. Gravitational force of rover is  $F_g \approx 1628$  N.

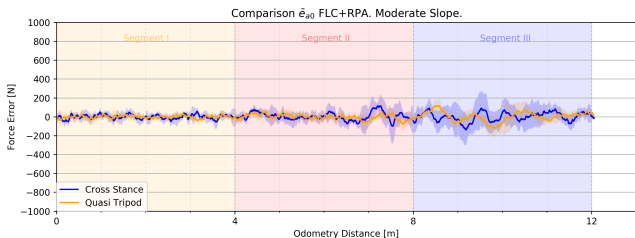
Footprint	GAP mode	$\hat{e}_{f0}$	$\hat{e}_{f1}$	$\hat{e}_{f2}$	$\hat{e}_{f3}$	$\hat{e}_{a0}$	$\hat{e}_{a1}$	$\hat{e}_r$	$\hat{e}_p$
	<i>noAdap</i>	229.18 N	236.76 N	223.00 N	233.83 N	455.91 N	455.91 N	1.39°	3.97°
	<i>FLCOnly</i>	40.31 N -82 %	35.91 N -85 %	34.71 N -84 %	40.61 N -83 %	34.30 N -92 %	34.30 N -92 %	1.24° -10 %	4.03° +1 %
	<i>FLC+RPA</i>	39.07 N -83 %	26.48 N -89 %	25.22 N -89 %	39.69 N -83 %	37.98 N -92 %	37.98 N -92 %	0.11° -92 %	0.10° -97 %
	<i>noAdap</i>	59.58 N	47.20 N	133.92 N	134.81 N	178.46 N	178.46 N	1.56°	3.98°
	<i>FLCOnly</i>	35.20 N -41 %	19.29 N -59 %	29.71 N -78 %	43.81 N -68 %	36.69 N -79 %	36.69 N -79 %	1.53° -2 %	3.95° -1 %
	<i>FLC+RPA</i>	38.08 N -36 %	16.01 N -66 %	25.71 N -81 %	44.43 N -67 %	33.19 N -81 %	33.19 N -81 %	0.20° -87 %	0.12° -97 %



(a) Contact axis FL-RR: Comparison between Cross-Stance and Quasi-Tripod without active ground adaption



(b) Contact axis FL-RR: Comparison between Cross-Stance and Quasi-Tripod with only FLC active



(c) Contact axis FL-RR: Comparison between Cross-Stance and Quasi-Tripod with FLC and RPA active

Figure 22: Force tracking errors in Moderate-Slope. Comparison of effects of GAP-modes and between two footprint configurations on FL-RR axis.

entation due to slip. The separate runs had different slip conditions and hence the trajectory on the slope might vary slightly from run to run. Furthermore, the runs are time/odometry based: More slip in one run leads to more time in steeper slope, which in turn increases the RMS value of the body angle. Activating the RPA module (Runs 6-9 and 12, 13) reduces both RMS errors,  $\hat{e}_r$  and  $\hat{e}_p$ , to below 1°. Again the error values in Run 6 are slightly higher than in the other runs due to the slip event causing the robot to shake for a period of time in mid-slope as described in Figures 20 and 26.

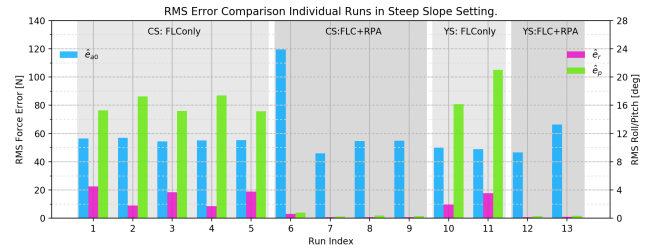


Figure 23: RMS error results of individual runs in Steep-Slope

#### 6.4.3 Conclusion: Force-Leveling and Body Angle Control Analysis

A simplified force leveling control was implemented for SherpaTT. In the experiments discussed above, an evaluation of different footprints in natural terrain was conducted to assess the generality of the simplifications for different footprints.

From the data presented, the force leveling control works comparable in different terrains and with different footprints. A clear improvement of the ground adaption in terms of force distribution is achieved with the force leveling control module. The errors between actual contact forces and expected contact forces are reduced by up to 92%. Absolute RMS errors for the contact forces are reduced well below 100 N for all runs in all footprints. In several settings, the errors were reduced to around 35 N, on the force-axes (common error for two wheels), compared to an overall gravitational force of  $F_g \approx 1628$  N. Error values that significantly differ from the range of values are explained by single events as for example active wheel unloading with jumps in reference

Table 14: RMS error values of forces, roll and pitch in of individual runs in Steep-Slope. Values from highlighted rows are plotted in Figure 23. Gravitational force of rover is  $F_g \approx 1628$  N.

idx														
	1	2	FLCOnly		5	6	FLC+RPA			9	FLCOnly		FLC+RPA	
			3	4			7	8			10	11	12	13
$\hat{e}_{f0}$	36.9 N	37.4 N	37.6 N	30.7 N	37.1 N	91.3 N	57.9 N	66.1 N	51.2 N		20.2 N	24.3 N	57.1 N	44.2 N
$\hat{e}_{f1}$	36.8 N	42.2 N	35.6 N	49.1 N	36.3 N	82.7 N	34.9 N	65.7 N	42.8 N		27.5 N	32.0 N	35.3 N	30.3 N
$\hat{e}_{f2}$	30.5 N	41.7 N	29.8 N	47.4 N	31.0 N	72.4 N	36.2 N	61.6 N	42.1 N		42.3 N	41.0 N	45.5 N	50.8 N
$\hat{e}_{f3}$	33.2 N	38.5 N	32.7 N	34.4 N	31.2 N	87.9 N	57.9 N	63.5 N	50.7 N		39.5 N	34.0 N	67.0 N	57.8 N
$\hat{e}_{a0}$	56.6 N	57.0 N	54.5 N	55.2 N	55.3 N	119.6 N	45.8 N	54.6 N	55.0 N		50.1 N	48.9 N	46.5 N	66.4 N
$\hat{e}_{a1}$	56.6 N	57.0 N	54.5 N	55.2 N	55.3 N	119.6 N	45.8 N	54.6 N	55.0 N		50.1 N	48.9 N	46.5 N	66.4 N
$\hat{e}_r$	4.5°	1.8°	3.7°	1.7°	3.8°	0.6°	0.1°	0.1°	0.2°		1.9°	3.6°	0.2°	0.2°
$\hat{e}_p$	15.3°	17.3°	15.2°	17.4°	15.1°	0.8°	0.3°	0.4°	0.3°		16.1°	21.0°	0.3°	0.3°

force values, causing temporary high error values.

Concerning the body angle control, RMS error values of both, roll and pitch angle were reduced to below  $0.5^\circ$  in all tested slopes and footprints with active RPA module. In moderate slopes the RMS errors are reduced to  $0.2^\circ$  or below.

With the experiments it was shown that a combined, multi-objective control is possible: The robot's wheel-ground contact forces can be controlled with simultaneous body roll-pitch angle control. Especially do FLC and RPA not influence each other, the force tracking quality does not change significantly between settings with or without active body roll-pitch control.

## 6.5 Terrain Slope Estimation

This section shows the results from validating the *Ground Plane Estimator* module presented in Section 5.1.

### 6.5.1 Presumption

The plane estimator fits a plane through all wheels with ground contact; using the time series of fitted planes, an estimation of the terrain profile the rover is driving on is possible. As only wheels with ground contact are used for the plane estimation, independence of the current footprint is expected. Hence, even when combining the runs from different GAP modes to one mean value, the respective standard deviation is expected to be low.

### 6.5.2 Results

Figure 24 shows the result of the slope estimation in Moderate-Slope. In the Subplots 24(a) and 24(b) the slope profile estimates of all forward and backward runs of a single footprint are combined to get a mean with standard deviation. Consequently, deviations for each footprint are calculated across the three types of runs (i) without active ground adaption (*noAdap*), (ii) only force leveling control active (*FLCOnly*), and (iii) force leveling together with roll-pitch adaption (*FLC+RPA*).

The highest deviations occur when the slope angle changes from increasing to decreasing and vice versa, hence when the rover enters or leaves the slope. Most likely this is due to slight inaccuracies in the synchronization of the individual runs which is based on odometry. Another reason for deviations in the plane estimates is to be found in the setting in a natural environment: Slight variations of the tracks driven in the individual runs can introduce variations in the actual slope profile the rover is driving on in the current experiment run.

Table 15 shows all maximum and mean deviation values of the runs in Moderate-Slope. Even though the settings of ground adaption modes are varying, the observable standard deviations are small, overall the mean deviation in the slope angle estimates is around one quarter of a degree. The maximum deviation in the slope profile height observed in all runs in Moderate-Slope is at 3 cm (Quasi-Tripod fwd) or 4.8% of the total estimated mean slope height (0.63 m).

From the plot of the slope angle estimates it can be seen that the terrain in Segment I has an incline around  $-1^\circ$  that increases before the rover enters Segment II. The locomotion distance is based on the front wheel pair, hence the slope angle is at the manually measured  $-8^\circ$  only when the rover is fully in Segment II. This is the case for approximately 6-8 m locomotion distance when driving forward and for 4-6 m locomotion distance when driving backwards, based on a wheel base  $w \approx 2$  m.

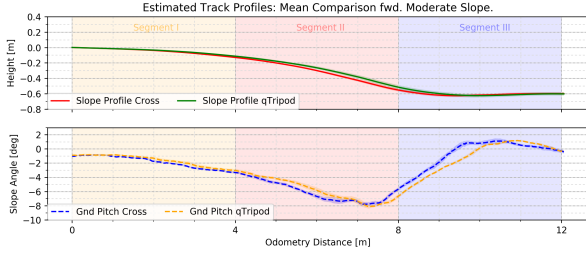
The results for the slope estimation in Steep-Slope are shown in Figure 25 in a similar manner as for Moderate-Slope. Since Steep-Slope was not conducted without active force leveling, the run means are composed from the ground adaption settings with

- only force leveling control active (*FLCOnly*), and
- force leveling together with roll-pitch adaption (*FLC+RPA*).

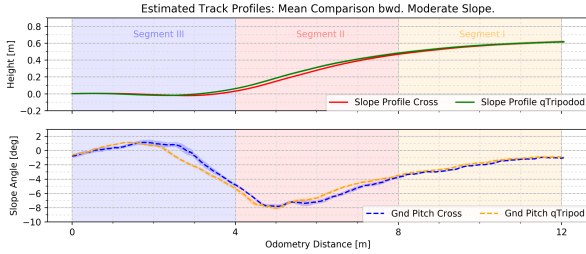
By building a mean over the runs with partially high slippage, high standard deviations are to be expected as the rover might not be at the same spot in the slope at each locomotion distance sample. In fact a wider

Table 15: Slope estimation experiment in Moderate-Slope. Maximum deviations over all runs of one footprint and RMS values of deviations.

Footprint	Slope pitch fwd		Slope pitch bwd		Slope profile fwd		Slope profile bwd	
	max( $\sigma$ )	RMS( $\sigma$ )	max( $\sigma$ )	RMS( $\sigma$ )	max( $\sigma$ )	RMS( $\sigma$ )	max( $\sigma$ )	RMS( $\sigma$ )
	0.46°	0.24°	0.57°	0.26°	0.02 m	0.01 m	0.02 m	0.01 m
	0.45°	0.22°	0.38°	0.19°	0.03 m	0.02 m	0.02 m	0.01 m



(a) Means and standard deviation of all runs with forward velocity. Driving starts in Front of Segment I.



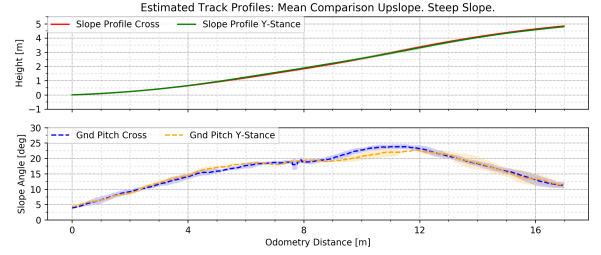
(b) Means and standard deviation of all runs with backward velocity. Driving starts in Segment III.

Figure 24: Test track profile from estimated plane in Moderate-Slope.

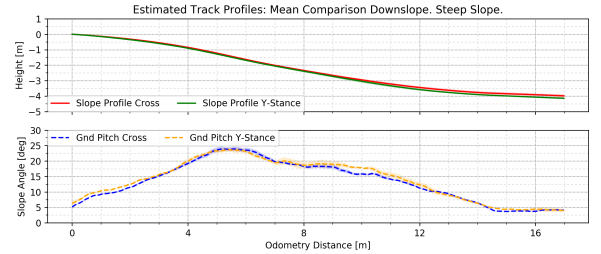
band of deviations can be seen around the slope pitch estimates, Table 16 lists the maximum deviations with up to 2.24°. However, the terrain profile estimates show relative small deviations with a maximum of 10 cm (Y-Shape upslope) which is corresponding to 2.1% of the total estimated mean slope height (4.79 m).

Comparing the estimated terrain profiles of upslope and downslope runs shows that the upslope runs estimate a higher terrain delta than the downslope runs. Manually measured was a height delta of 4.73 m, the estimate for upslope in Cross-Stance is 4.84 m, and in Y-Shape 4.79 m; while downslope estimates are -3.98 m and -4.14 m, respectively. The reason for this is slippage in the slope: Upslope slippage leads to a longer amount of time/odometry distance in steeper parts of the slope, while this is the opposite while driving down the slope. However, in similar terrain, the estimation yields similar results, hence a systematic error due to slippage can be identified in the terrain estimates.

In Figure 25(a) a jump in the mean value for the ground pitch estimation in Cross-Stance can be seen at approximately 7.5 m locomotion distance. The jump is caused by a temporary loss of ground contact of the front left wheel due to slip in Run 6. The wheel without ground



(a) Slope estimation uphill runs in Steep-Slope



(b) Slope estimation downhill runs in Steep-Slope

Figure 25: Slope estimation with slip in Steep-Slope.

contact is excluded from the ground plane calculation, hence a jump in the plane estimate occurs. The data from the single run is plotted in Figure 26.

### 6.5.3 Conclusion: Slope Estimation Analysis

From the data subsumed in Tables 15 and 16, it can be confirmed that the terrain estimation is invariant of the footprint. Furthermore, the small deviations for the means over different GAP-modes show that it is also independent of the chosen adaption mode.

However, since the module relies on proprioceptive data only (forward kinematics of legs and IMU measurements), the influence of the footprint, more precisely the wheel base, is always present in the measurements: The footprints used in the experiments have a different baseline in forward/backward-direction of the rover. While the baseline is  $w_{cs}=2.04$  m for Cross-Stance, the difference between front and rear wheel pair is  $w_{qtp}=2.29$  m for Quasi-Tripod configuration and  $w_{ys}=2.30$  m for Y-Shape.

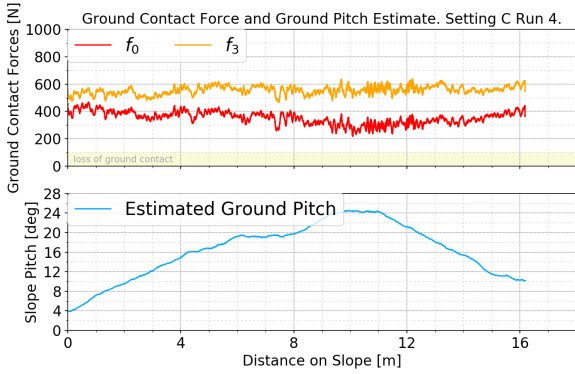
The effect of this difference can be found when comparing the slope estimates. Consequently, different footprints can result in different ground plane estimates for a given path on natural terrain. The deviation values are comparable between the different footprints, indicating

Table 16: RMS values slope estimation experiment in Steep-Slope.

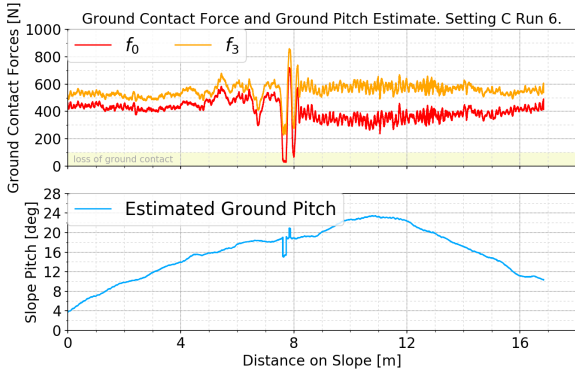
Footprint	Slope pitch up		Slope pitch dwn		Slope profile up		Slope profile dwn	
	max( $\sigma$ )	RMS( $\sigma$ )	max( $\sigma$ )	RMS( $\sigma$ )	max( $\sigma$ )	RMS(dev)	max( $\sigma$ )	RMS(dev)
	1.81°	0.94°	0.85°	0.41°	0.10 m	0.06 m	0.09 m	0.06 m
	2.24°	1.03°	1.33°	0.64°	0.10 m	0.05 m	0.09 m	0.05 m

a similar performance independent of the footprint.

As shown in Steep-Slope with higher slip ratios than in Moderate-Slope, the slippage of the system has an impact on the ground plane estimate, which is currently based on the odometry of the system. Slip when driving up a slope leads to a higher ground plane estimate than actually travelled, while driving down the slope with skid leads to a lower ground plane estimate.



(a) Run 4 in Steep-Slope. Regular slip in slope, all wheels with permanent ground contact: Constant ground plane angle estimate.



(b) Run 6 in Steep-Slope. Heavy Slip (100%) in the middle of the slope leads to loading and unloading of the wheels. Loss of ground contact for front left wheel around 7.5 m into the slope leads to exclusion of this wheel in ground plane estimate and hence to a jump in the estimated plane pitch angle.

Figure 26: Comparison of regular run and run with heavy slip: Forces FL and RR and Estimated ground pitch angle.

## 6.6 Slope Climbing

The slope climbing experiments in Steep-Slope are used to identify an influence of ground adaption mode and/or footprint on the climbing abilities of SherpaTT in natural terrain.

### 6.6.1 Presumption

For the slope climbing ability it is expected, that shifting the CoG to the front wheels (the “upslope-wheels”) has a positive influence on the slippage of the system. Hence, for the tested footprint Y-Shape a better result is expected.

The main investigation in this test is based on the slip/skid data which is calculated from the difference of odometry and DGPS-data. Following definition is used for slippage analysis:

$$s = 1 - \frac{d_{gps}}{d_{odo}}, \quad (13)$$

where  $d_{gps}$  is the travelled distance on slope as recorded by the gps-system and  $d_{odo}$  is the locomotion distance as output from odometry. When  $s > 0$ , the odometry distance is greater than the gps distance, hence the rover was subject to slip, which is expected to happen during the upslope runs. When  $s < 0$ , the odometry distance is smaller than the gps distance, hence the rover was skidding, which might happen mostly during downslope drives. By normalizing with the odometry distance, the final  $s$  value is always normalized by 17 m, while the GPS distance is different depending on slip and skid events during each run.

### 6.6.2 Results

Figure 27 shows an overview of the results for the two footprints Cross-Stance and Y-Shape. Plotted are the means of  $d_{odo}$  over the means of  $d_{gps}$  for all runs of one

footprint regardless of the ground adaption mode but separated into uphill and downhill runs. Ideally without slip or skid,  $d_{odo} = d_{gps}$ , thus the values would be on the  $45^\circ$  line indicated in both plots. However, the plots show that the uphill runs are subject to slip (red line), while the downhill runs are subject to skid. Uphill the slippage starts around  $d_{gps} \approx 6-8$  m, which is around the beginning of the steepest part of the slope (see Table 5). The uphill plots for both footprints become roughly parallel to the  $45^\circ$  line at about  $d_{gps} \approx 12$  m, meaning that the slip is close to zero, only the accumulated slip is still present. A slope distance of 12 m is approximately when the front wheel pair leaves the steepest part of the slope in uphill runs.

In the downhill runs (rover driving backwards), skid starts after around  $d_{gps} \approx 2$  m which means the front wheels enter segment 14-15 while the rear wheels leave segment 13-14 (wheel base of roughly 2 m). At around  $d_{gps} \approx 12$  m, the plot is more or less parallel to the  $45^\circ$  line, indicating close to zero skidding in that part of the slope, which is the 4-5 m segment from Table 5 for the front wheels, thus when the rover is past the steepest part of the slope.

Table 17 lists the final slip/skid values according to Equation (13). In the case of combining all up- and downhill runs of one footprint no significant difference between the footprints can be found. Overall both footprints seem to be working similar on the tested slope, where the Cross-Stance shows a slightly better performance. Both footprints perform better in downhill than in uphill runs.

The results when splitted according to the GAP-mode are presented in the right part of the table. Activating the roll-pitch adaption degrades the results for both footprints in uphill runs, while it improves the results of the downhill runs.

The development of the slip/skid values over driven distance is plotted in Figure 28. Since the plotted slip value is dependent on  $\frac{d_{gps}}{d_{odo}}$  the value  $s$  decreases for phases without slip during the traverse. Note that, in the beginning, small values ( $<1$  m) for  $d_{gps}$  and  $d_{odo}$ , in combination with sensor noise cause high fluctuation in the values.

When comparing the same GAP-settings in different footprints, a similar development of the slip/skid values over the traverse can be found. Most prominent is the case for *FLC+RPA* when driving downslope. Both plots have nearly the same development and end up with a total skid ratio of -6.5% and -7%, respectively. The least similar plots are for the case *FLC+RPA* in upslope runs: In Y-Shape, the rover has less slip in the beginning of the slope but has a massive slippage event around 9 m of odometry distance. However, in the end the slippage is similar for both footprint configurations. Note that for both cases, uphill and downhill, each plot for Y-Shape is based on a single run, while the plots for Cross-Stance are the mean of two runs. These results indicate that the GAP-mode seems to have a higher influence on the slope climbing ability than the footprint.

Consequently, a clear distinction of a favorable footprint for slope climbing is not possible from the data gained in these experiments. Using the combined up/down power requirements from Table 10, it seems that a Cross-Stance is slightly favorable for downslope drives and a Y-Shape is slightly favorable for upslope driving.

### 6.6.3 Conclusion: Slope Climbing Analysis

The conducted experiments in Steep-Slope setting show that the robot is able to cope with natural terrain with up to  $28^\circ$  inclination. All presented runs were successful runs in terms of climbing the slope and reaching the top of the hill with reduced velocity.

However, as stated in Section 6.1.3, runs with a velocity of 0.1 m/s were successful only before the duri-crust on the slope was broken. With lose soil on the slope and velocity setting  $\dot{x} = 0.1$  m/s, the rover ended with 100% slip in the steepest part, the runs had to be aborted.

Two different footprints are analysed for the slope climbing. Neither in terms of slip nor in terms of energy consumption there is a significant difference between both footprints observable. Comparing the applied GAP modes, a slightly increased power requirement for active roll-pitch adaption with decreased upslope climbing performance is observable when compared to only force leveling active. Hence, *FLConly* mode should be preferred when a defined body orientation is not required.

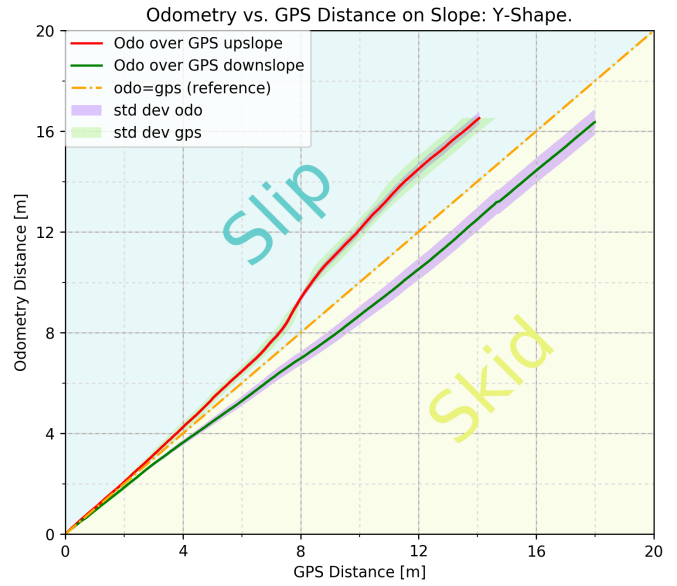
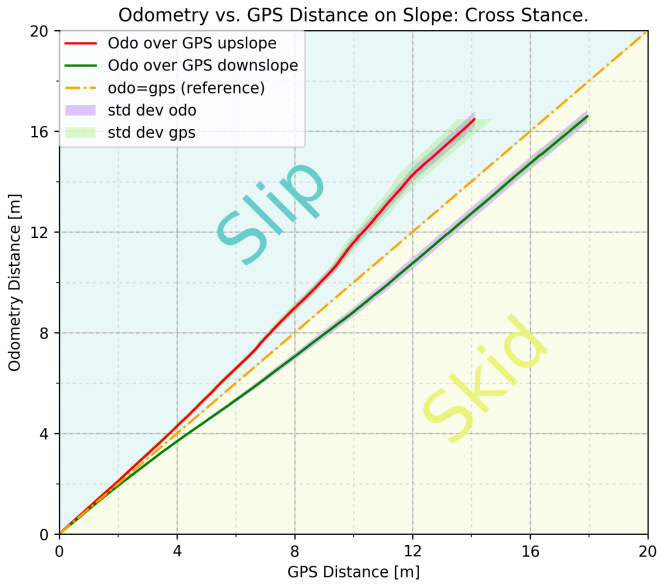
In Turtle-Front footprint, structural loads seemed to endanger the robot's integrity. This assessment was done based on the optical impression of the rover in the slope, runs in this footprint were skipped for safety reasons.

## 7 Conclusion and Future Work

This paper presents the development and an in-field evaluation of the hybrid wheeled-leg rover system SherpaTT. SherpaTT is developed for usage in a heterogeneous multi-robot exploration system with modular components. The main focus of this paper is the electro-mechanical design of the rover and its locomotion performance. A four week field deployment was conducted in the desert of Utah, USA to validate the system in natural terrain. The results of this outdoor field campaign extend the former indoor laboratory experimental results published in (Cordes and Babu, 2016) and (Cordes et al., 2017).

The rover is equipped with four identical suspension units ("legs") that are used for active ground adaption. Each leg has five active DoF, three of which are mainly used for ground adaption and body roll-pitch control, while two are used to steer and drive the wheel at the end of the leg.

To achieve a coherent behavior in rough terrain, a Motion Control System (MCS) for SherpaTT is introduced. The MCS takes in motion, body posture and footprint



(a) Overall slippage in Cross-Stance up (red) and down (green).

(b) Overall slippage in Y-Shape up (red) and down (green).

Figure 27: Odometry distance vs. GPS distance on slope. Means over all adaption modes.

Table 17: Slip (positive) and skid (negative) values for runs in Steep-Slope.

Footprint	Combined		Separated according to GAP-mode			
	Upslope	Downslope	Up <i>FLCOnly</i>	Up <i>FLC+RPA</i>	Dwn <i>FLCOnly</i>	Dwn <i>FLC+RPA</i>
 CS	+14.3%	-8.2%	+10.2%	+18.5%	-9.2%	-6.5%
 YS	+14.8%	-10.1%	+10.1% <sup>*)</sup>	+19.5% <sup>*)</sup>	-13.1% <sup>*)</sup>	-7.0% <sup>*)</sup>

<sup>\*)</sup> single run values

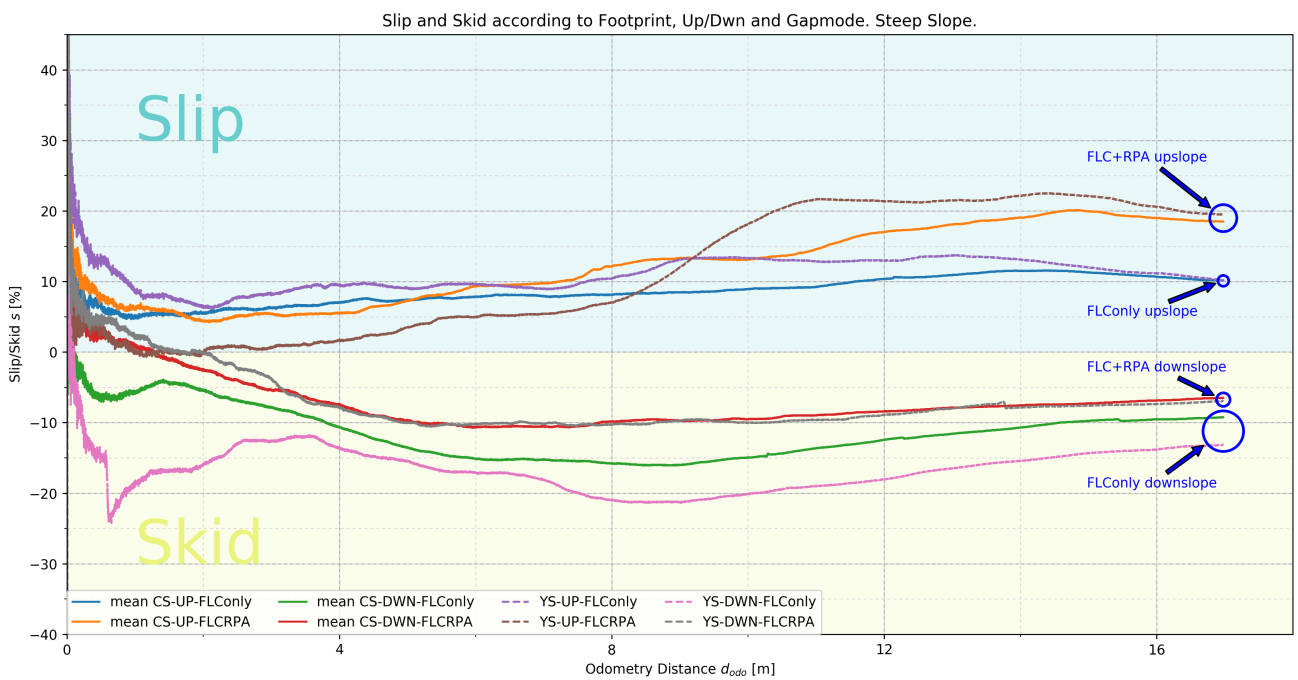


Figure 28: Slip/Skid values separated by footprint, movement direction and GAP-mode.

commands as well as force and body roll-pitch measurements. From these inputs, a coordination of the legs is realized with the goal of permanent wheel-ground contact with optimal force balancing. Optionally the body’s roll-pitch angle can be controlled in natural terrain. The force balancing presented in this paper is optimal in terms of the to-be-expected forces at each wheel resulting from the current footprint and the position of the center of mass within the support polygon spanned by the wheels with ground contact.

In the field tests, the rover was driven through three different terrain categories, ranging from mostly flat terrain over moderate slopes to a steep slope with up to 28° inclination covered with loose soil and duri crust. In each terrain set, different footprints and combinations of active GAP modes were tested. The data gathered from these runs is analysed with emphases on (i) energy consumption for locomotion/active ground adaption, (ii) reference force tracking and body roll-pitch control, (iii) ground plane estimation, and (iv) slope climbing abilities in steep slopes.

The experiments showed that the suspension system with its 12 active DoF is not the main power consumer during locomotion. The four wheels and four steering actuators that are also required for passive suspension systems are responsible for the majority of power consumption. Main increase in absolute power requirement from flat terrain to steep slopes is resulting from the drive system, while the suspension system’s power requirement is more related to “roughness” of terrain. The test tracks in the presented experiments are rather smooth; in undulating terrain, the power draw of the suspension is expected to increase. This will be quantified in upcoming experimental setups.

In terms of Force Leveling Control (FLC), the presented experiments show that the FLC component is capable of coping with different footprints. The component is able to keep all wheels in ground contact and reduce the force tracking RMS error down to as low as 16 N for individual wheels (gravitational force of the rover:  $F_g \approx 1628 \text{ N}$ ). Additionally activating the roll-pitch adaption does not impede the results of the FLC component, while being able to reduce the roll-pitch tracking RMS errors to below 0.5° in all settings (one run with heavy slippage and robot body oscillations showed RMS errors of  $\hat{e}_r = 0.6^\circ$  and  $\hat{e}_p = 0.8^\circ$ , though).

The ground plane estimation from proprioceptive data showed to have very small deviations across footprints and GAP-modes. Slippage and skidding down slopes, however, affects the results of the plane estimation. The data indicates that the effects are reproducible, in further developments of SherpaTT the proprioceptive ground plane estimates could be used to refine exteroceptive data originating from lidar or camera data and vice versa. Using the plane estimate together with a WCP estimation on the circumference of the wheel, improvements in LEP positioning for active ground adaption are aspired for future work.

From the slope climbing experiments it can be con-

firmed, that the rover can climb natural terrain slopes with up to 28° inclination. From the data of the experiments it seems that the choice of the GAP-modes has a higher influence than the choice of the footprint on the slippage conditions in the slope. If not required, the RPA-mode should be preferably inactive in slope climbing.

Further analysis of the data shows that changing the pitch angle in the slope gives more workspace and additionally has an influence on the reference forces generated by FLC. This analysis is not presented in detail in this paper, more investigation is needed to realize a reference force balancer by manipulating the reference pitch in an adequate way, this is left for the future work on the system.

Currently also in development is an active leg movement for steering support. When a new steering reference occurs, a trajectory for the LEP shall be generated, that ensures a smooth position and velocity trajectory for the WheelSteering joint without high deltas between current angle and new reference angle.

Additionally the realization of virtual 3D springs for each leg is currently being investigated. Using the force vector measured at each wheel, a virtual compliance can be realized. The effects of this virtual spring on the locomotion shall be investigated in future works.

Finally, evaluation of a combination of reactive control and planning algorithms is aspired. A three dimensional model of the environment can be generated using SherpaTT’s lidar scanner. A trajectory for each LEP and the body’s center can then be planned in the terrain map. Reactive control then only needs to accommodate for model inaccuracies, while the knowledge of the terrain profile ahead might improve the response-time in ground adaption.

## Acknowledgments

The authors would like to thank the *TransTerra* and *FT-Utah* team members and supporting staff at the DFKI Bremen Robotics Innovation Center. Special acknowledgement is due for the efforts of Leif Christensen, Steffen Planthaber, Thomas M. Roehr, Roland U. Sonsalla, and Tobias Stark of the field team in Utah. Without the joint effort of all field team members, the experiments would not have been possible to conduct. The projects *TransTerra* and *FT-Utah* are funded by the German Space Agency (DLR, Grant number: 50RA1301 and 50RA1621) with federal funds of the Federal Ministry of Economics and Technology (BMWi) in accordance with the parliamentary resolution of the German Parliament.

## References

Advanced Navigation (2017). Spacial dual datasheet. <http://www.advancednavigation.com.au/sites/advancednavigation.com.au/files/>

Spatial%20Dual%20Datashet.pdf, last call 2017-09-19.

- Apfelbeck, M., Ku, S., Rebele, B., Michaud, S., Boesch, C., Krpoun, R., and Schfer, B. (2011). Exomars phase b2 breadboard locomotion sub-system test campaign. In *Proceedings of Advanced Space Technologies for Robotics and Automation, (ASTRA'11)*.
- Azkarate, M., Zwick, M., Carrio, J. H., Nelen, R., Wiese, T., Joudrier, P. P. A., and Visentin, G. (2015). First experimental investigations on wheel-walking for improving triple-bogie rover locomotion performances. In *Proceedings of Advanced Space Technologies for Robotics and Automation, (ASTRA'15)*.
- Balme, M., Curtis-Rouse, M., Banham, S., Barnes, D., Barnes, R., Bauer, A., Bedford, C., Bridges, J., Butcher, F., Caballo, P., Caldwell, A., Coates, A., Grindrod, C., Gunn, M., Gupa, S., Hansen, R., Harris, J., Holt, J., Huber, B., Huntly, C., Hutchinson, I., Jackson, L., Kay, S., Kyberd, S., Lerman, H., McHugh, M., McMahon, W., Muller, J.-P., Paar, G., Preston, L., Schwenzer, S., Stabbins, R., Tao, Y., Traxler, C., Turner, S., Tyler, L., Venn, S., Walker, H., Wright, J., and Yeomans, B. (2017). UK Space Agency 'Mars Utah Rover Field Investigation 2016' (MURFI 2016): Overview of Mission, Aims and Progress. In *Proceedings of the Lunar Planetary Science XLVIII*.
- Bartlett, P., Wettergreen, D., and Whittaker, W. L. (2008). Design of the scarab rover for mobility and drilling in the lunar cold traps. In *International Symposium on Artificial Intelligence, Robotics and Automation in Space (i-SAIRAS'08)*.
- Bartsch, S., Cordes, F., Haase, S., Planthaber, S., Roehr, T. M., and Kirchner, F. (2010). Performance evaluation of an heterogeneous multi-robot system for lunar crater exploration. In *Proceedings of the 10th International Symposium on Artificial Intelligence, Robotics and Automation in Space (iSAIRAS'10)*, Sapporo, Japan.
- Bartsch, S., Manz, M., Kampmann, P., Dettmann, A., Hanff, H., Langosz, M., v. Szadkowski, K., Hilljegerdes, J., Simnofske, M., Kloss, P., Meder, M., and Kirchner, F. (2016). Development and control of the multi-legged robot mantis. In *Proceedings of ISR 2016: 47th International Symposium on Robotics*, pages 1–8.
- Bickler, D. B. (1989). Articulated suspension system. US-Patent US4840394 (A) – 1989-06-20 <https://ntrs.nasa.gov/search.jsp?R=19900007837>. Last access: 2018-02-06.
- Caudill, C., Galofre, A. G., Pontefract, A., and Osinski, G. (2016). 2015 CANMARS MSR Analog Mission: In situ geochemical insights from x-ray fluorescence spectrometry. In *Proceedings of the 47th Lunar and Planetary Science Conference*.
- Clarke, J. D. and Stoker, C. R. (2011). Concretions in Exhumed and Inverted Channels near Hanksville Utah: Implications for Mars. *International Journal of Astrobiology*, 10(3):161–175.
- Cordes, F. and Babu, A. (2016). SherpaTT: A versatile hybrid wheeled-leg rover. In *Proceedings of the 13th International Symposium on Artificial Intelligence, Robotics and Automation in Space (iSAIRAS 2016)*.
- Cordes, F., Babu, A., and Kirchner, F. (2017). Static force distribution and orientation control for a rover with an actively articulated suspension system. In *Proceedings of the 2017 IEEE/RSJ International Conference on Intelligent Robots and Systems (IROS 2017)*, Vancouver, Canada.
- Cordes, F., Dettmann, A., and Kirchner, F. (2011). Locomotion modes for a hybrid wheeled-leg planetary rover. In *Proceedings of the IEEE International Conference on Robotics and Biomimetics (IEEE-Robio 2011)*, Phuket, Thailand.
- Cordes, F., Oekermann, C., Babu, A., Kuehn, D., Stark, T., and Kirchner, F. (2014). An active suspension system for a planetary rover. In *Proceedings of the International Symposium on Artificial Intelligence, Robotics and Automation in Space (iSAIRAS 2014)*, Montreal, Canada.
- Dettmann, A., Roemmermann, M., and Cordes, F. (2011). Evolutionary development of an optimized manipulator arm morphology for manipulation and rover locomotion. In *Proceedings of the IEEE International Conference on Robotics and Biomimetics (IEEE-Robio 2011)*.
- Dupuis, E., Picard, M., Haltigin, T., Lamarche, T., Rocheleau, S., and Gingras, D. (2016). Results from the csa's 2015 mars analogue mission in the desert of utah. In *Proceedings of the 13th International Symposium on Artificial Intelligence, Robotics and Automation in Space (i-SAIRAS'16)*, Beijing, China.
- Gingras, D., Allard, P., Lamarche, T., Rocheleau, S. G., Gemme, S., and Picard, M. (2017). Overview of the 2016 canadian mars sample return analogue deployment and the technology behind. In *Proceedings of the 14th Symposium on Advanced Space Technologies in Robotics and Automation (ASTRA'17)*.
- Haarmann, R., Jaumann, R., Claasen, F., Apfelbeck, M., Klinkner, S., Richter, L., Schwendner, J., Wolf, M., and Hofmann, P. (2012). Mobile payload element (mpe): Concept study for a sample fetching rover for the ESA lunar lander mission. *Planetary and Space Science*, 74(1):283 – 295. Scientific Preparations For Lunar Exploration.
- Harrington, B. D. and Voorhees, C. (2004). The challenges of designing the rocker-bogie suspension for the mars exploration rover. In *In 37th Aerospace Mechanisms Symposium*.

- Haynes, G. C., Stager, D., Stentz, A., Vande Weghe, J. M., Zajac, B., Herman, H., Kelly, A., Meyhofer, E., Anderson, D., Bennington, D., Brindza, J., Butterworth, D., Dellin, C., George, M., Gonzalez-Mora, J., Jones, M., Kini, P., Laverne, M., Letwin, N., Perko, E., Pinkston, C., Rice, D., Scheifflee, J., Strabala, K., Waldbaum, M., and Warner, R. (2017). Developing a robust disaster response robot: Chimp and the robotics challenge. *Journal of Field Robotics*, 34(2):281–304.
- Heverly, M., Matthews, J., Frost, M., and McQuin, C. (2010). Development of the tri-athlete lunar vehicle prototype. In *Proceedings of the 40th Aerospace Mechanisms Symposium*, NASA Kennedy Space Center.
- Huntsberger, T., Stroupe, A., Aghazarian, H., Garrett, M., Younse, P., and Powell, M. (2007). Tressa: Teamed robots for exploration and science on steep areas. *Journal of Field Robotics*, 24(11-12):1015–1031.
- Iagnemma, K., Rzepniewski, A., Dubowsky, S., and Schenker, P. (2003). Control of robotic vehicles with actively articulated suspensions in rough terrain. *Autonomous Robots*, 14(1):5–16.
- Kroemer, O., Beermann, D., Cordes, F., Lange, C., Littau, B., Rosta, R., Scharringhausen, M., van Zoest, T., and Grimm, C. (2011). Adaptive flexible wheels for planetary exploration. In *Proceedings of the 62nd International Astronautical Congress (IAC2011)*, Cape Town.
- Krotkov, E., Hackett, D., Jackel, L., Perschbacher, M., Pippine, J., Strauss, J., Pratt, G., and Orłowski, C. (2017). The darpa robotics challenge finals: Results and perspectives. *Journal of Field Robotics*, 34(2):229–240.
- Lamon, P. and Siegwart, R. (2003). 3d-odometry for rough terrain - towards real 3d navigation. In *2003 IEEE International Conference on Robotics and Automation (Cat. No.03CH37422)*, volume 1, pages 440–445.
- Lindemann, R. and Voorhees, C. (2005). Mars exploration rover mobility assembly design, test and performance. In *IEEE International Conference on Systems, Man and Cybernetics, 2005*, volume 1, pages 450–455 Vol. 1.
- Manz, M., Dettmann, A., Hilljegerdes, J., and Kirchner, F. (2012). Development of a lightweight manipulator arm using heterogeneous materials and manufacturing technologies. In *Proceedings of the International Symposium on Artificial Intelligence, Robotics and Automation in Space (i-SAIRAS 2012)*; September 4-6, Turin, Italy. o.A.
- Manz, M., Sonsalla, R. U., Hilljegerdes, J., Oekermann, C., Schwendner, J., Bartsch, S., and Ptacek, S. (2014). Design of a rover for mobile manipulation in uneven terrain in the context of the spacebot cup. In *Proceedings of the International Symposium on Artificial Intelligence, Robotics and Automation in Space (i-SAIRAS'14)*.
- Michaud, S., Gibbesch, A., Thueer, T., Krebs, A., Lee, C., Despont, B., Schfer, B., and Slade, R. (2008). Development of the exomars chassis and locomotion subsystem. In *Proceedings of i-SAIRAS 2008 - 9th International Symposium on Artificial Intelligence, Robotics and Automation in Space*.
- Michaud, S., Schneider, A., Bertrand, R., Lamon, P., Siegwart, R., van Winnendael, M., and Schiele, A. (2002). SOLERO : Solar Powered Exploration Rover. In *None*.
- Mishkin, A., Morrison, J., Nguyen, T., Stone, H., Cooper, B., and Wilcox, B. (1998). Experiences with operations and autonomy of the mars pathfinder microrover. In *Aerospace Conference, 1998 IEEE*, volume 2, pages 337–351 vol.2.
- Mumm, E., Farritor, S., Pirjanian, P., Leger, C., and Schenker, P. (2004). Planetary cliff descent using cooperative robots. *Autonomous Robots*, 16(3):259–272.
- Nenas, I. A., Matthews, J. B., Abad-Manterola, P., Burdick, J. W., Edlund, J. A., Morrison, J. C., Peters, R. D., Tanner, M. M., Miyake, R. N., Solish, B. S., and Anderson, R. C. (2012). Axel and duaxel rovers for the sustainable exploration of extreme terrains. *Journal of Field Robotics*.
- Reid, W., Prez-Grau, F. J., Gktoan, A. H., and Sukkarieh, S. (2016). Actively articulated suspension for a wheel-on-leg rover operating on a martian analog surface. In *2016 IEEE International Conference on Robotics and Automation (ICRA)*, pages 5596–5602.
- Roehr, T. M., Cordes, F., and Kirchner, F. (2014). Reconfigurable integrated multirobot exploration system (RIMRES): Heterogeneous modular reconfigurable robots for space exploration. *Journal of Field Robotics*, Special Issue on Space Robotics, Part 2:3–34.
- Schenker, P. S., Huntsberger, T. L., Pirjanian, P., Baumgartner, E., Aghazarian, H., Trebi-ollennu, A., Leger, P. C., Cheng, Y., Backes, P. G., Tunstel, E. W., Propulsion, J., and Dubowsky, L. S. (2001). Robotic automation for space: Planetary surface exploration, terrain-adaptive mobility, and multi-robot cooperative tasks. In Hall, D. P. C. E. L., editor, *Intelligent Robots and Computer Vision XX: Algorithms, Techniques, and Active Vision*, volume 4572, pages 12–28, Boston, MA, USA.
- Smith, P. (2004). The phoenix mission to mars. In *Aerospace Conference, 2004. Proceedings. 2004 IEEE*, volume 1, page 342 Vol.1.
- Sonsalla, R., Cordes, F., Christensen, L., Planthaber, S., Albiez, J., Scholz, I., and Kirchner, F. (2014). Towards a Heterogeneous Modular Robotic Team in a Logistic Chain for Extraterrestrial Exploration. In *Proceedings of the International Symposium on Artificial Intelligence, Robotics and Automation in Space (i-SAIRAS 2014)*. International Symposium on Artificial Intelligence, Robotics and Automation in Space.

- Sonsalla, R. U., Cordes, F., Christensen, L., Roehr, T. M., Planthaber, S., Stark, T., and Kirchner, E. (2017). Field trials to demonstrate a cooperative multi-robot mission in mars analogue environment. In *Proceedings fo the 14th Symposium on Advanced Space Technologies in Robotics and Automation (ASTRA'17)*.
- Thueer, T., Lamon, P., Krebs, A., and Siegwart, R. (2006). Crab - exploration rover with advanced obstacle negotiation capabilities. In *Proceedings of the 9th ESA Workshop on Advanced Space Technologies for Robotics and Automation (ASTRA'08)*.
- Townsend, J., Biesiadecki, J., and Collins, C. (2010). Athlete mobility performance with active terrain compliance. In *Aerospace Conference, 2010 IEEE*, pages 1–7.
- Volpe, R. (2005). Rover technology development and mission infusion beyond mer. In *Aerospace Conference, 2005 IEEE*, pages 971–981.
- Welch, R., Limonadi, D., Samuels, J., Warner, N., and Morantz, C. (2013). Verification and validation of mars science laboratory surface system. In *System of Systems Engineering (SoSE), 2013 8th International Conference on*, pages 64–69.
- Wenzel, W., Cordes, F., and Kirchner, F. (2015). A robust eletro-mechanical interface for cooperating heterogeneous multi-robot teams. In *Proceedings of the 2015 IEEE International Conference on Intelligent Robots and Systems (IROS-15)*, pages 1732–1737, Hamburg.
- Wettergreen, D., Jonak, D., Kohanbash, D., Moreland, S. J., Spiker, S., Teza, J., and Whittaker, W. L. (2009). Design and experimentation of a rover concept for lunar crater resource survey. In *47th AIAA Aerospace Sciences Meeting Including The New Horizons Forum and Aerospace Exposition*.
- Wilcox, B., Litwin, T., Biesiadecki, J., Matthews, J., Heverly, M., Morrison, J., Townsend, J., Ahmad, N., Sirota, A., and Cooper, B. (2007). Athlete: A cargo handling and manipulation robot for the moon. *Journal of Field Robotics*, 24(5):421.
- Wilcox, B. H. (2012). Athlete: A limbed vehicle for solar system exploration. In *2012 IEEE Aerospace Conference*, pages 1–9.